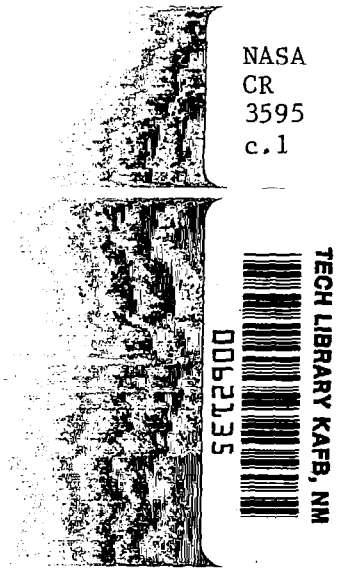

NASA Contractor Report 3595

A Frost Formation Model and Its Validation Under Various Experimental Conditions

Mark A. Dietenberger

CONTRACT NAS8-33369
AUGUST 1982

NASA

NASA Contractor Report 3595

A Frost Formation Model and Its Validation Under Various Experimental Conditions

Mark A. Dietenberger
University of Dayton
Dayton, Ohio

Prepared for
Marshall Space Flight Center
under Contract NAS8-33369

National Aeronautics
and Space Administration

Scientific and Technical
Information Branch

1982

ACKNOWLEDGEMENT

This research was sponsored by the National Aeronautics and Space Administration, Marshall Space Flight Center, Space Sciences Laboratory, Atmospheric Sciences Division, under Contract NAS8-33369. The author is indebted to Mr. A. Richard Tobiason of the Office of Aeronautics and Space Technology, NASA Headquarters for support of this research and Mr. Dennis Camp of Marshall Space Flight Center for his assistance as Technical Monitor.

TABLE OF CONTENTS

LIST OF ILLUSTRATIONS

LIST OF TABLES

LIST OF SYMBOLS

$\frac{dx_{s_0}}{dt}$ is the ice needle growth rate in the initial frost layer

g is the gravitational acceleration (m/s^2)

h_H is the convective heat transfer coefficient ($w/m^2°K$)

h_M is the convective mass transfer (g/m^2s)

h^*_M is the enhanced mass transfer coefficient due to boundary layer fogging (g/m^2s)

jlw is the water vapor flux at the plate surface from the air

jqw is the convective heat flux at the plate surface from the air

k_a is the thermal conductivity of air ($w/m°K$)

k_s is the aerodynamic sand-grain roughness height (m)

$\dot{m}_d$ is the water vapor diffusion flux inside the layer (g/m^2s)

$\dot{m}_{d_s}$ is the water vapor diffusion flux entering the frost layer (g/m^2s)

q is the heat flux given by equation (13) (w/m^2)

t is the time (s)

u is the air boundary layer velocity parallel component

x is the distance from the plate surface (m) (or parallel distance in Appendix III)

x_s is the frost thickness (m)

x_{s_o} is the height of the ice needle in the initial frost layer (m)

$\frac{x_{s_o}}{t}$ is the approximated ice needle growth rate in the initial frost layer (m/s)

y is the distance from the plate surface in Appendix III (m)

B is the frost porosity

C_f is the local friction coefficient

C_1 is the fitting constant in equation (9)

C_o is a fitting constant in equation (3)

C_f is the specific heat of air (1.005 J/g)

D is the diffusion coefficient as a function of air temperature and ambient pressure

D_e is the haydraulic diameter of a duct (m)

Gr_H is the Grashof number defined by equation (24)

H is the length from the plate leading edge to the frost formation location (m)

H_o is the convective and radiative heat flux (w/m^2)

K is the frost thermal conductivity ($w/m°K$)

L_e is the latent heat of evaporation (2500 J/g)

L_s Is the latent heat of sublimation (2834.2 J/g)

Nu is the Nusselt number

Nu_D is the Nusselt number based on cylinder diameter

Nu_x is the local Nusselt number

Pr is the Prandtl number

P_v is the water vapor pressure

Q_o is the heat flux through the ice needle of the initial frost layer (w/m^2)

$Q_o - H_o$ is the latent heat flux release (w/m^2)

Re Is the Reynolds number

Re_D is the Reynolds number based on hydraulic diameter or cylinder diameter

Re_x is the local Reynolds number

R_v is the gas constant of water vapor

S is the saturation ratio for fog nucleation

Sc is the Schmidt number

Sh is the Sherwood number

St_x is the local Stanton number

T is the frost interior temperature (°K)

T_a is the air temperature (°K)

T_{dp} is the dew-point temperature (°K)

T_f is the fog-point temperature (°K)

T_{fp} is the frost point temperature (°K)

T_s is the frost surface temperature (°K)

T_{s_o} is the ice needle surface temperature (°K)

T_w is the plate wall temperature (°K)

T_∞ is the blackbody ambient temperature

V_w is the normal velocity at the condensing surface

W is the weighting factor for a condensing surface

δ is the air momentum boundary layer thickness

δ_t is the air thermal boundary layer thickness

ε_I is the blackbody emissivity of ice

n is defined by equation (23)

ν is the kinematic viscosity (m^2/s)

ξ is the boundary layer thickness ratio between the thermal thickness and the momentum thickness

ρ_a is the air density (g/m^3)

ρ_{fo} is the initial frost density (g/m^3)

ρ_I is the ice density (.917g/cc)

ρ_{vs} is the saturated water vapor density at the frost surface temperature (g/m)

σ is the Steffan-Bottzmann constant

τ_s is the tortuosity factor (1.1)

ϕ is the angular deviation of the plate from the vertical direction

ϕ_a is the ambient relative humidity ratio

χ is the water vapor mass fraction

ω_a is the ambient absolute humidity

ω_s is the saturated absolute humidity at the frost surface temperature

ω_{s_a} is saturated absolute humidity at air temperature

ω_w is saturated absolute humidity at wall temperature

ϕ is defined by equation (26)

θ is the angular deviation from the stagnation point

τ_w is the surface shear stress

FROST FORMATION MODELING APPLIED TO VARIOUS DATA SETS

SECTION 1
INTRODUCTION

Frost formation commonly occurs when a surface in the presence of humid air is cooled to temperatures below 0°C and below the dew-point. In the field of refrigeration and air-conditioning this phenomenon has an adverse effect upon heat transfer and pressure loss, thus leading to lower efficiencies. In aerospace technology frost creates safety hazards. For instance, in the northern climates, aircraft takeoffs can be hazardous if nocturnal frost is present on the airfoil. Another technology concerned with frost is that of the space shuttle. A frost layer on the external cryogenic tanks of the space shuttle could shear off at launch and damage the orbiter tiles. The emerging cryogenic technology in other industries is very likely to experience similar concerns with frost formation.

Frost formation is a complicated transient process in which a variety of heat and mass transfer mechanisms are at work simultaneously. It can be characterized as having three regimes. In the first regime, the initial frost layer can begin in one of two ways. In the first case initial condensation occurs at nucleation sites on the wall resulting from a critical super-saturation. In the other case (for a very cold wall) boundary layer fogging occurs and the fog becomes the major source for water droplet condensation on the wall. Thus the "frost-point" temperature (i.e., the temperature at which frost actually begins to form) lies somewhere between the fog-point temperature and the dew-point temperature, depending on nucleation sites on the wall and on the wall temperature. The "frost-point" temperature is an especially important consideration for nocturnal frost formation. Some initial frost properties such as density and thickness need

to be calculated, because of the processes described above, in order to move on to the next regime of frost formation.

The second regime is dominated by vapor diffusion from the air boundary layer into the macroscopic frost layer. This process increases the average frost density. As the frost grows in thickness, the insulating effect of the frost layer causes an increase in the frost surface temperature. This in turn causes a decrease in the mass flux, which consists of both vapor flux and fog droplets flux in the boundary layer, as well as a decrease in the heat flux. The frost layer thickness also increases when the mass flux from the boundary layer is larger than the diffusional mass flux entering the frost layer. Boundary layer fogging may disappear (depending on the frost surface temperature) since the fog droplets are assumed to freeze on the frost surface. Generally, since the thermal conductivity of the frost increases along with frost density, this regime is characterized by a feedback effect in which the frost surface temperature slowly increases as the frost layer grows.

After a while a third regime is reached. The frost surface temperature becomes a constant, thus giving a steady-state heat flux in the boundary layer. The phenomena of liquid water seepage, in addition to the water vapor diffusion, from the frost surface into the interior of the frost need to be considered in order to explain the constant frost surface temperature. An effect that remains mysterious, but has been acknowledged by many investigators is that, at least on a flat plate, the frost density at any time tends to be uniform throughout the frost layer, although the density increases with time. The spatially uniform frost density can not be completely explained by a vapor diffusion model. One possible explanation assumes a thermal diffusion process of water or ice particles within the frost layer. No one has yet constructed a model based on such a process, however. The assumption of a spatially uniform frost density has been utilized in the frost formation model described in this report.

In classic work, Brian, et al. [1] and Brian, et al. [2] chose a diffusional model approach to calculate the frost density and thickness as a function of time. They used a heat balance at the frost surface to calculate the frost surface temperature. Then by assuming the frost surface is saturated and the frost density is spatially uniform, the rate of frost density change was related to the temperature gradient at the frost surface. Finally, the difference between the boundary layer vapor mass flux and the diffusional mass flux into the frost could be used to calculate the frost thickness.

When the Brian model is closely examined, one discovers certain limitations. First, in the heat balance equation, the frost thermal conductivity is only applicable at wall temperatures of 80°K and with a high initial saturation ratio, as demonstrated by Dietenberger [3]. Second, the heat and mass transfer coefficients of the boundary layer are not very well known, particularly in relationship to the roughness of the frost surface. Chen and Rohsenow [4] showed that the heat and mass transfer coefficients are affected by the frost surface roughness. Third, the calculation of frost density and thickness is dependent on an effective numerical integration scheme which also requires fairly good initial values of frost density and thickness. Finally, there are no provisions for the quasi-steady state phase, where the frost surface temperature reaches a constant. Because the diffusional approach lends itself to time-varying meteorological conditions, Jones and Parker [5] applied Brian's et al. method and achieved partial success in predicting frost thickness trends, even when humidity and/or velocity changed during an experimental run.

Due to the complicated nature of frost growth, other early investigators attempted an empirical approach to the frost density prediction without relying on a physical model. A significant effort was made by Biguria and Wenzel [6] to correlate frost

density on a flat plate with air stream velocity, air stream humidity, plate temperature, nature of the boundary layer, and the frost surface temperature. Lotz [7] used a different data set to derive yet a different correlation of the frost density with frost thickness, air stream velocity, air stream temperature, and the vapor pressure difference between the air and frost. Lastly, Parish and Sepsy [8] used a simple correlation of the frost density with frost surface temperature to calculate the frost growth on a cylinder in conjunction with a laminar boundary layer/potential flow method. Without any explanation of a physical model of frost density, it was not imperative to apply the frost density correlations to the model of frost growth in general.

Recently, some investigators who used the quasi-steady state assumption were able to postulate a physical model of frost thickness growth. In the quasi-steady state assumption the frost surface temperature or the heat flux eventually reaches a constant value, although the frost density and thickness will continue to increase. If the frost grows long enough, the frost surface eventually reaches 0°C, providing that the air stream temperature and the dew-point are above freezing temperature. In experiments for forced convection over a cylinder, Schneider [9] observed that frost thickness tends to be independent of the Reynold's number and the vapor pressure difference between the air stream and the frost. Consequently, he formulated frost thickness according to the principles of crystal growth. Treating a frost crystal as a vertical cylinder, the heat flux of condensation was equated with the heat flux of conduction through the cylinder. This resulted in a frost thickness growth written as the square roots of the time and of the temperature difference between the frost surface and the wall. This basic model was empirically corrected by including the effects of supersaturation and the condensation soaking of the porous frost structure. Schneider then used five other references containing experimental

data on cylinders to claim that the generality of his correlation for the frost thickness was independent of the geometrical shape of the flow channel as well as of the kind of flow. In this paper we will show that Schneider's correlation is valid for his own data set, but not in agreement with other data selected for review.

In a more basic development, White [10] used thermal conductivity as a linear function of the frost density and as an arbitrary function of the frost interior temperature. By invoking the quasi-steady heat flux assumption and integrating the frost thermal conductivity across the frost thickness, the overall frost density became a linear function of the frost thickness. This operation was then combined with the mass balance at the frost surface, and spatially invariant frost density was assumed, resulting in frost thickness as an analytic function of time, mass flux to the frost surface, the initial frost density and thickness, the wall and frost surface temperatures, and the coefficients of the thermal conductivity. White found that for the range of experimental data observed, there was a very small dependence on the wall and frost surface temperatures and the coefficients of the thermal conductivity. From these observations he concluded that half the mass flux is deposited on the frost surface and the other half goes into the frost to increase the frost density. We note that these correlations were limited to low frost densities and are only applicable to the quasi-steady regimes of frost growth.

This paper describes a numerical model that has been used to calculate the frost properties for all regimes of frost growth. In the first regime of frost growth, the initial frost density and thickness was modeled from the theories of crystal growth, similar to Schneider's approach. The "frost-point" temperature was modeled as a linear interpolation between the dew-point temperature and the fog-point temperature, based upon the nucleating capability of the particular condensing surface.

For a second regime of frost growth, the diffusional model of Brian, et al. was adopted with the following enhancements: the generalized correlation of the water frost thermal conductivity from Dietenberger was applied to practically all water frost layers in place of Brian's, et al. correlation, being careful to ensure that the calculated heat and mass transfer coefficients agreed with experimental measurements of the same coefficients. In particular, the heat transfer coefficient was enhanced due to the roughness of the frost layer and the mass transfer coefficient was enhanced due to the boundary layer fogging. Finally, an efficient and accurate numerical integration scheme was developed to calculate the frost surface temperature and the frost density and thickness as a function of time. The numerical scheme responded to changes in environmental conditions, with good agreement to Jones and Parker's data.

In the third regime of frost growth, the frost surface temperature was held fairly constant by a procedure described as the water seepage model, which is explained later in this paper. Agreement with experimental data for the quasi-steady regime was superior to that obtained using Schneider's or White's correlations.

SECTION 2
THE FROST INITIATION MODEL

The wall temperature at which the frost begins to form is the frost-point temperature, which is determined by the equation,

$$T_{fp} = WT_{dp} + (1 - W)T_f \qquad (1)$$

The dew-point temperature and the fog-point temperature equations are presented in Appendix I.

Once the frost begins to form, we assume the initial frost layer will grow according to the principles of crystalization. Following Schneider [9] the frost layer is modeled as cylindrical ice needles growing away from the wall. The one-dimensional conductive heat flux through the ice needle is assumed balanced by the various heat flux contributions from the air to the ice crystal. The surface temperature of the ice needle is assumed to be at the dew-point temperature but not greater than the freezing temperature. The heat flux terms are different than those assumed by Schneider. The steady state conductive heat flux through the ice crystal is given by

$$Q_o = \frac{630}{T}\frac{dT}{dx} = \frac{630}{X_{s_o}} \ell n(T_{s_o}/T_w) \qquad (2)$$

This heat flux is balanced by the heat flux from the air to the ice as,

$$Q_o = C_o L_s \rho_I \left(\frac{\omega_{s_a} - \omega_w}{\omega_a - \omega_w}\right)^n \left(\frac{dx_{s_o}}{dt}\right) + H_o \qquad (3)$$

$$H_o = h_H\left(T_a - T_{s_o}\right) + \alpha\varepsilon_I\left(T_\infty^4 - T_{s_o}^4\right) \qquad (4)$$

In Schneider's approach, n is 1/2 and H_o is zero, which worked well for thick frost layers. The classical nucleation theory requires n=1 for an ice needle isolated from other

needles, as would be expected in an initial frost layer. As will be demonstrated later, H_o turns out to be small compared to Q_o. Solving for the ice needle height or the initial frost thickness, X_{s_o}, we obtain by integration from equations (2) and (3) and with n=1,

$$\left(\frac{-K_o}{C_o L_s \rho_I}\right)\left(\frac{\omega_a-\omega_w}{\omega_{s_a}-\omega_w}\right) t = \left(\frac{K_o}{H_o}\right)^2 \ell n\left(1-\frac{H_o}{K_o} x_{s_o}\right)+ \frac{K_o}{H_o} x_{s_o} \qquad (5)$$

where

$$K_o = 630 \ell n(T_{s_o}/T_w) \qquad (6)$$

During the short time needed for the initial frost layer to develop, the mass flux to the frost layer from the air is approximated as,

$$h_m(\omega_a-\omega_w) \simeq (1-B)\rho_I\left(\frac{x_{s_o}}{t}\right) \qquad (7)$$

Combining equations (5), (6), and (7), we obtain the frost density as a function of x_{s_o}, as,

$$\rho_{f_o} = \rho_a - (\rho_I - \rho_a)\left(\frac{C_o h_m L_s}{H_o}\right)(\omega_{s_a} - \omega_w)\left[1 + \frac{Q_o}{H_o}\ell n\left(1- \frac{H_o}{Q_o}\right)\right]. \qquad (8)$$

In order to estimate a value for x_{s_o} so that ρ_{f_o} can be calculated, we use the approximation

$$\ell n(1-x) \simeq -x-\frac{1}{2}x^2$$

in equation (5) to explicitly solve for x_{s_o} as

$$x_{s_o} = C_1\left[\left(\frac{\omega_a-\omega_w}{\omega_{s_a}-\omega_w}\right) \ell n(T_{s_o}/T_w)\right]^{1/2} \qquad (9)$$

and

$$C_1 = \frac{1260\ t_o}{c_o L_s \rho_I} . \qquad (10)$$

The terms C_o and C_1 are fitting constants obtained from the data reviewed in this paper. The nominal values for C_o and C_1 are 15.56 and 0.001. Equations (8) and (9) allow us to solve for the initial frost density and thickness; that is, the thickness and density at the end of the crystal growth dominated regime. These values are inputs to the diffusion dominated regime modeling. It turned out that the values of initial frost density and thickness did not have to be very accurate because the diffusion growth model generates most of the frost layer. Thus at times far removed from the initial time, the frost thickness and density are not very sensitive to the intial values of frost density and thickness.

SECTION 3

THE FROST FORMATION MODEL

The basic approach for modeling frost growth in the diffusion dominated regime follows that of Brian, et al. except for differences in the various terms of the equations. When the heat flux, which includes latent, convective, and radiative transport from the air to the frost surface, is made equal to the conductive heat flux through the frost layer at the frost surface, the temperature of the frost surface can be calculated. The frost surface temperature will change with time because the frost layer becomes denser and thicker, which in turn affects the computations of the heat flux in the frost layer. During the process of frost formation it is assumed that the part of the water vapor and all of boundary layer fog droplets transported to the surface freeze at the surface, thus increasing the thickness of the frost. The remaining water vapor is diffused into the existing frost layer before it freezes. Since the frost density is assumed to be spatially invariant in a direction normal to the plate, the water vapor diffusion flux entering the frost surface from the surrounding air is given by

$$\dot{m}_{ds} = \frac{\partial(1-B)}{\partial t}\rho_I x_s \qquad (10)$$

where $\dot{m}_{ds}$, ρ_I, and x_s stand for water vapor diffusion mass flux at the surface, ice density, and frost thickness respectively. B is the porosity of the frost. Also, the water vapor mass flux, $\dot{m}_d$, will obey the diffusion equation and will be driven by the temperature gradient throughout the frost layer.

The water diffusion flux is given by equation (8) from Dietenberger,

$$\dot{m}_d = \frac{DB}{(1-\chi)\tau_s}\ \frac{P_v}{R_v T^2}\left(\frac{L_s}{R_v T} - 1\right)\frac{dT}{dx} \quad . \qquad (11)$$

Equation (11) can be evaluated at the frost surface if the frost surface temperature, T_s, the frost surface temperature gradient, $\left.\frac{dT}{dx}\right|_s$, and the frost thickness x_s are known. Combining equations (10) and (11) allows the frost density to be solved for as a function of time.

To obtain a value for frost surface temperature, T_s, the quasi-steady-state heat equation for the frost layer is to be solved. That is, the equation

$$K\frac{dT}{dx} = q \tag{12}$$

with the frost thermal conductivity, K, given by equation (23) from Dietenberger (reproduced in Appendix II) is to be solved with the boundary conditions

$$T = T_s \text{ at } x = x_s \quad \text{and} \quad T = T_w \text{ at } x = 0,$$

where

$$q = h_H (T_a - T_s) + h_m L_s (\omega_a - \omega_s) + \varepsilon\sigma (T_a^4 - T_s^4) \quad . \tag{13}$$

This gives

$$\int_{T_w}^{T_s} K \, dT = x_s \, q \quad . \tag{14}$$

The temperature gradient at the frost surface is given by

$$\left.\frac{dT}{dx}\right|_s = \frac{q}{K(T_s)} \quad . \tag{15}$$

The thickness of the frost can be computed from the ice portion of the frost $(1-B)\rho_I x_s$ which is directly related to the mass transfer coefficient and the water vapor humidity by

$$\frac{d[(1-B)\rho_I x_s]}{dt} = h_m(\omega_a - \omega_s) \tag{16}$$

Since these equations cannot be solved analytically, numerical techniques are used to solve these equations to obtain the thickness and the density of the frost.

The numerical scheme begins by assuming a small initial value of frost density, ρ_{fo} and frost thickness, x_{so}, obtained from equations (8) and (9).

The frost surface temperature, T_s, is obtained from the monotonic nonlinear equation (14). In order to solve equation (14) in an accurate and efficient manner, the frost thermal conductivity, K, in equation (14) is first interpolated by a parabolic function in a temperature range ΔT and integrated to get the first term in equation (14) (i.e., ΔT is often greater than $T_s - T_w$). Then T_s in equation (14) is solved for by an interval-halving-iterative technique so that the left term of equation (14) is equal to the right terms. In this way successive evaluations of the complicated thermal conductivity expression, K, and numerical integrations can be completely avoided when iterating to get T_s. The temperature gradient at the frost surface is obtained by equation (15). The value for the frost density is predicted for a later time, t_{n+1}, by combining equations (10) and (11) to get $\partial\rho_f/\partial t$, which is solved by using a second order Runge Kutta "initial" scheme and by a second order predictor-corrector "takeover" scheme. An accurate predictor equation was adapted from White's [10] analytic form for the frost density. Finally, the value for the frost thickness is predicted for the same time as the frost density (i.e., at t_{n+1}) by integrating equation (16), where the rectangular rule is used for the integration, in acknowledgement of the fact that h_m and ω_s are slowly changing functions of time. At the same time, a new frost surface temperature is calculated by returning to equation (14), incrementing n, and using the new values of frost density, ρ_f, and thickness, x_s.

The regime of the quasi-steady state where the frost surface temperature is held constant is modeled in the following

way. If at a particular time, t_n, the frost surface temperature, T_s, as solved by the previously described method, goes above a critical temperature, hereafter known as the water seepage temperature, then the numerical scheme is altered to let the frost thickness be a constant in the time interval t_n to t_{n+1} and the frost density is computed by the integration of equation (16) over the interval t_n to t_{n+1}. Thus liquid water seeps into the frost layer, increasing its density but not affecting the thickness. The time is incremented and the frost surface temperature, T_s, is solved from equation (14) and is again compared to the water seepage temperature, and so on. Altering the frost growth in this manner has the effect of keeping the frost surface temperature constant. Generally the water seepage temperature tends to be lower than or equal to 273.16°K in order to gain agreement with the data presented later. It is postulated that some isolated regions of the frost surface are at 273.16°K while the other regions are below the water seepage temperature, which when the region temperatures are averaged out gives the frost surface temperature. Thus, for very cold wall temperatures the water seepage is expected to be somewhat less than freezing while for wall temperatures approaching freezing the water seepage temperature would nearly equal the freezing temperature.

The frost formation model as described above need not be restricted to flat plate frost formation. The model can be applied to any geometrical surface including curved surfaces as long as the wall temperature and the heat and mass transfer coefficient distribution can be provided.

SECTION 4
COMPARISON TO EXPERIMENTAL DATA

The validity and generality of the frost formation model has been demonstrated by comparison with several different data sets appearing in the literature. Each set of published data required separate derivations of the convective heat and mass transfer coefficients depending on whether the air flow was forced or natural, in a duct, on a cylinder, laminar or turbulent, etc. Each data set contained the appropriate values needed for input into the frost formation model. These values include wall temperature, air temperature, relative humidity, airspeed, and the apparatus dimensions. In addition, many published data sets also presented measurements of both frost weight and thickness. Other published data just contained the frost thickness. For the latter data sets, a very accurate mass transfer coefficient was needed to compensate for the lack of a frost weight measurement.

For each data set presented, the analysis of the convective heat and mass transfer coefficient will be discussed first. Then a table of input values to the frost formation model will be presented for that data set. Finally the corresponding frost model prediction of frost weight and thickness will be compared to the experimental observations and an evaluation provided. The published data examined were from Brian et al. [2], Brian, et al. [1], Yamakawa, et al. [11], Jones and Parker [5], Okino and Tajima [12], Schneider [9], Andrichak [13] and White [10].

4.1 TURBULENT FORCED CONVECTION IN A DUCT

Most of the data sets analyzed were frost formation experiments performed in a duct with turbulent forced convection. These included Brian et al. [2], Brian, et al. [1], Yamakawa, et al., and Jones and Parker.

In Brian, et al. [2] and Brian et al. [1] experimental runs, the boundary layer temperature profiles were not fully developed but were fully turbulent. In other words the entrance effects of the duct were affecting the heat and mass transfer but were not affecting the momentum transfer. For the Yamakawa, et al. experiments the boundary layer temperature profiles were both fully developed and fully turbulent. The air velocities and duct dimensions of the Jones and Parker experimental runs are similar to Yamakawa et al., thus leading to similar conclusions as Yamakawa et al., concerning boundary layer temperature and velocity profiles. The simplicity of the flow conditions allows one to use the Nusselt and Sherwood number correlations commonly used in the general literature for the calculation of heat and mass transfer coefficients. In particular, Yamakawa et al. used the popular Colburn equation,

$$Nu = 0.023\ Re^{0.8} Pr^{1/3} = h_H D_e / k_a . \qquad (17)$$

for the Nusselt number, Nu, as a function of Reynold's number, Re, based on the hydraulic diameter, D_e, and the Prandtl's number, Pr. This curve is plotted in Figure 1.

The Sherwood number is usually obtained via the Chilton-Colburn analogy, from the Nusselt number as

$$Sh = Nu(Sc/Pr)^{1/3} = \frac{h_m D_e}{\rho_a D_a} \qquad (18)$$

or equivalently equations (17) and (18) can be rewritten in terms of heat and mass transfer coefficient ratio as

$$h_H/h_m = C_p(Pr/Sc)^{-2/3} . \qquad (19)$$

These relationships assume that the duct walls are smooth and clean and that the boundary layer temperature and velocity profiles are fully developed and fully turbulent. In the Yamakawa, et al. case these assumptions were questionable and therefore Yamakawa et al. checked experimentally to make

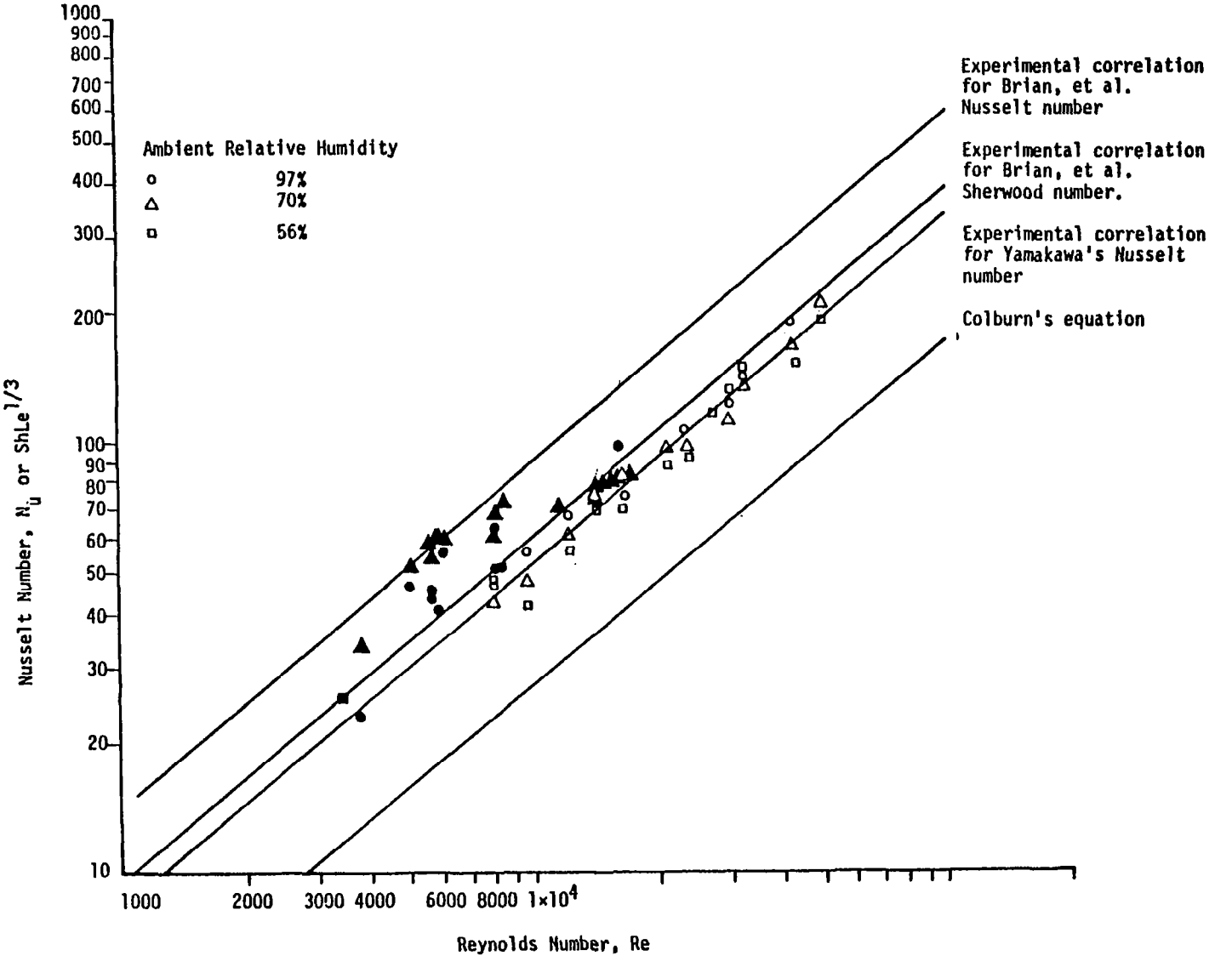

Figure 1. Correlation of the Experimental Nusselt's Number Containing the Heat Transfer Coefficient, h_H^*, versus Reynolds Number.

sure that Colburn's equation for the Nusselt number equation was still valid. Their results in Figure 1 show that the right hand term of equation (17) must be increased by a factor 1.95, which then must be explained. One possible explanation is an increase in heat transfer due to the surface roughness of frost. It was determined that two other possible causes of heat transfer enhancement--the boundary layer fogging effect on temperature profile, and the boundary layer transpiration as related to the vapor mass flux divided by the bulk flux--are nil.

There is evidence that the heat transfer coefficient is affected by the frost surface roughness. This problem of frost roughness was taken up by Chen and Rohsenow [4] who did frost formation in cylindrical tubes. They attempted to calculate the aerodynamic roughness height of the frost layer and then calculate the corresponding increase in the heat transfer coefficient. Using the relative correction to h_H from Yamakawa as 1.95, one can use the equations from Chen and Rohsenow to show that the approximate aerodynamic roughness height of Yamakawa's data can be related as $k_s \simeq x_s/0.6$. This is the value of aerodynamic roughness due to frost recommended by Langston [15] in his studies of hoar frost on airplane wings. Thus surface roughness appears to be a reasonable explanation of enhanced heat transfer coefficients.

Yamakawa, et al. also experimentally checked to see if the Chilton-Colburn's analogy between the heat and mass coefficients was valid for their experiments. Figure 2 shows their plot of the experimental heat and mass transfer coefficients. They did not relate their data to relative humidity or Reynolds number as was done in Figure 1. Yamakawa's data points lie above the relationship given by equation (19). On the other hand, the rough wall heat transfer coefficient is greater, by a factor of

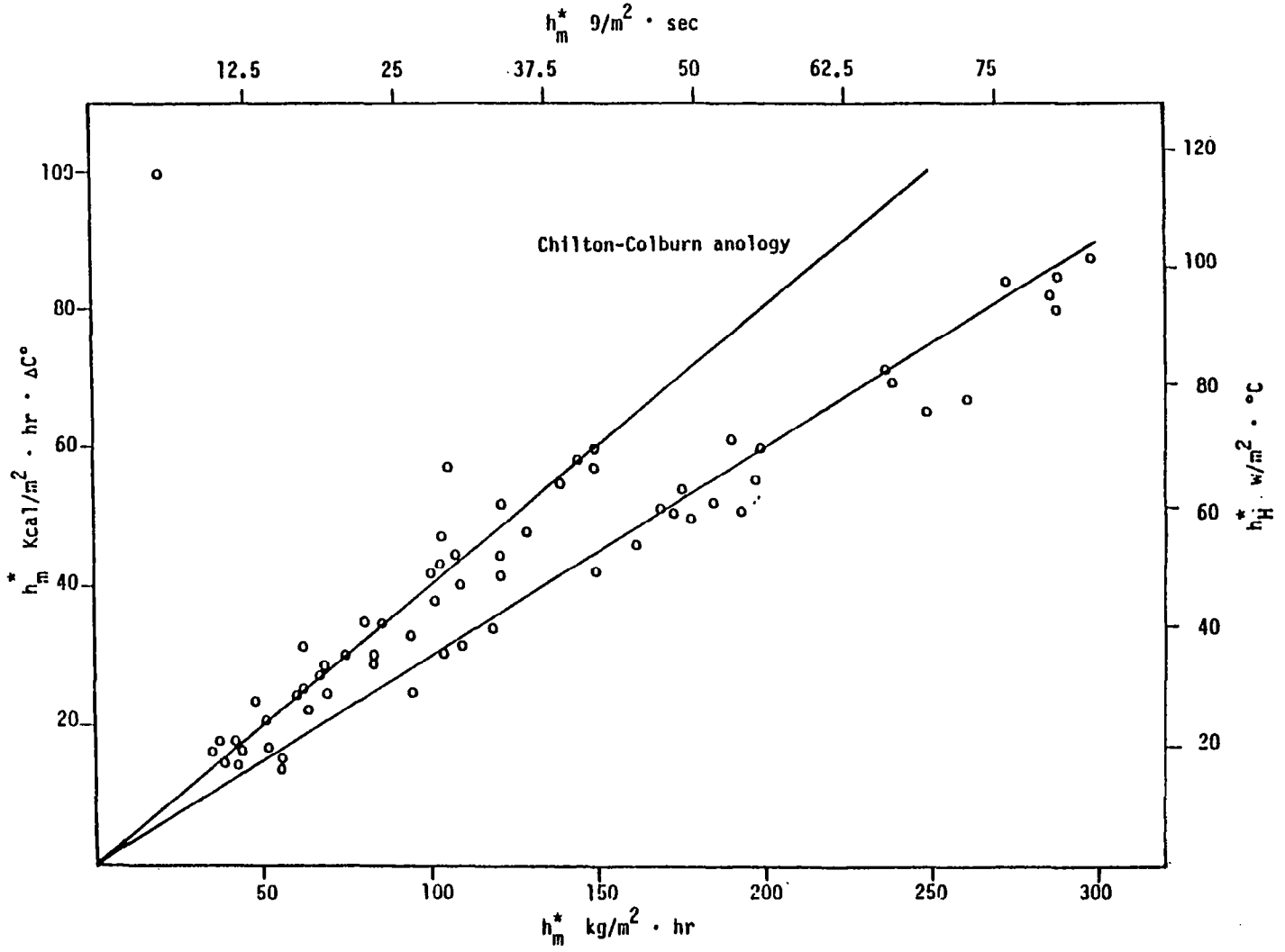

Figure 2. Correlation of the Experimental Heat Transfer Coefficient, h_H^*, versus the Experimental Mass Transfer Coefficient, h_m^*. (Data obtained from Yamakawa, et al.).

analogy relationship to the rough wall heat transfer coefficient. This resulted in the upper line in Figure 2. The lower line was obtained by using the constant 1.5 instead of 1.95.

If one proposed an enhancement in the mass transfer coefficient due to the boundary layer fogging as an explanation for the lower line in Figure 2, then the mass transfer enhancement averages out to 1.95/1.5 = 1.3. This is approximately the value typically predicted when boundary layer fogging is considered, as is done in the model (see Appendix I).

Thus we conclude that to make sense of Yamakawa's data for the heat and mass transfer coefficients, the smooth wall heat transfer coefficient must be increased by the roughness factor 1.95 and the smooth wall mass transfer coefficient increased by the mass transfer enhancement equation due to the boundary layer fogging. From Street [16] and Yaglom and Kader [17] we find that, at least for the fully rough flow, a basic analogy exists between the heat and mass transfer coefficients. This means if the Yamakawa et al. data is in the fully rough regime, then our conclusion could be invalid. However, using equations for the friction coefficient from Chen and Rohsenow and a roughness height of $k_s = X_s/0.6$, we find that the Yamakawa et al. data was clearly in the transitionally rough regime, where a heat and mass transfer analogy does not apply.

A similar analysis of the heat and mass transfer coefficients for Brian et al. [2] data shows the same type of conclusion, with one additional factor necessary to correct for the thermal entrance length of the duct. The single solid square point in Figure 1 replotted from Brian et al. [2] is the smooth wall Nusselt number measurement, which is 2.24 higher than the Colburn equation at the same Reynold's number. This is due to the thermal entrance effects of the duct as discussed by Brian et al. [2]. Also non-dimensionalized and replotted from Brian, et al. [2] is the analogy of the Nusselt number via equation (18),

the Sherwood number times the one-third power of the Lewis number. These are given by the solid dots in Figure 1, which then shows that the mass transfer coefficient via the Sherwood number corresponds to the smooth wall case, allowing for the mass transfer enhancements due to boundary layer fogging.

On the other hand, the heat transfer coefficient via the Nusselt number (corresponding to the solid triangle in Figure 1) shows a correlation of 3.36 higher than the Colburn's equation (ignoring the Reynolds number at around 1.5×10^4) or 1.51 greater than the smooth wall Nusselt number correlation. Using the factor 1.51 for the relative increase in the heat transfer coefficient due to frost roughness and using equations from Chen and Rohsenow we also find that the Brian et al. data are clearly in the transitionally rough regime. Thus these data sets, in the transitionally rough regime, demonstrate the following behavior of the heat and mass transfer coefficients: the mass transfer coefficient shows a smooth wall behavior in the transitionally rough regime and the heat transfer coefficient shows a rough wall behavior in the same regime.

At this point, the only other information needed for input to the numerical frost formation model of turbulent forced convection in a duct is the specification of ambient conditions such as Reynold's number, absolute humidity, wall temperature, and air temperature. Since the frost formation model was adapted from Brian, et al. [1] we first compared the numerical predictions with Brian, et al. [2] data. Initially their time frames were translated to correspond to the zero time of frost formation rather than the zero time of their run. Table I provides a list of input data into the numerical frost formation model and Figures 3 and 4 show the corresponding calculations of frost thickness and the frost mass per area (here defined as frost weight) respectively from zero time of frost formation. The frost thickness data in Figure 3 shows a lot of scatter but on the average the model predicted the frost thickness fairly well.

TABLE I
DATA INPUT TO THE FROST FORMATION MODEL FOR COMPARISON
WITH BRIAN ET AL. [2] DATA FOR FORCED CONVECTION IN A DUCT

Computer Curve No.	Experimental Graph Symbol	Reynolds Number	Absolute Humidity	Wall Temperature (°K)	Air Temperature (°K)
1	○	5100	0.0031	79.83	307.05
2	△	5790	0.0031	79.83	297.60
3	□	8000	0.00357	79.83	297.60
4	●	8430	0.0035	79.83	284.27

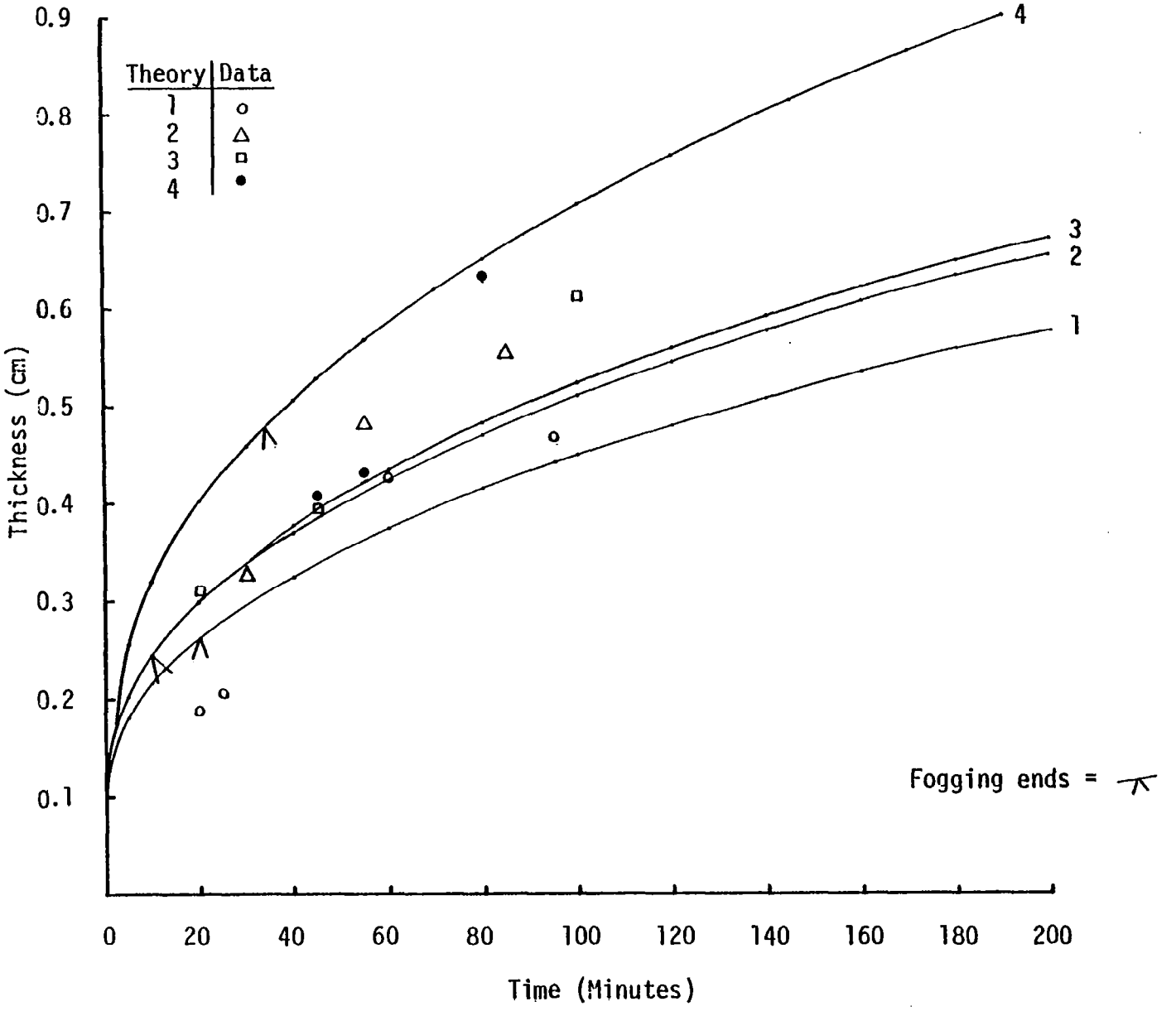

Figure 3. Frost Thickness versus Time for Brian, et al. Data (Reference 2).

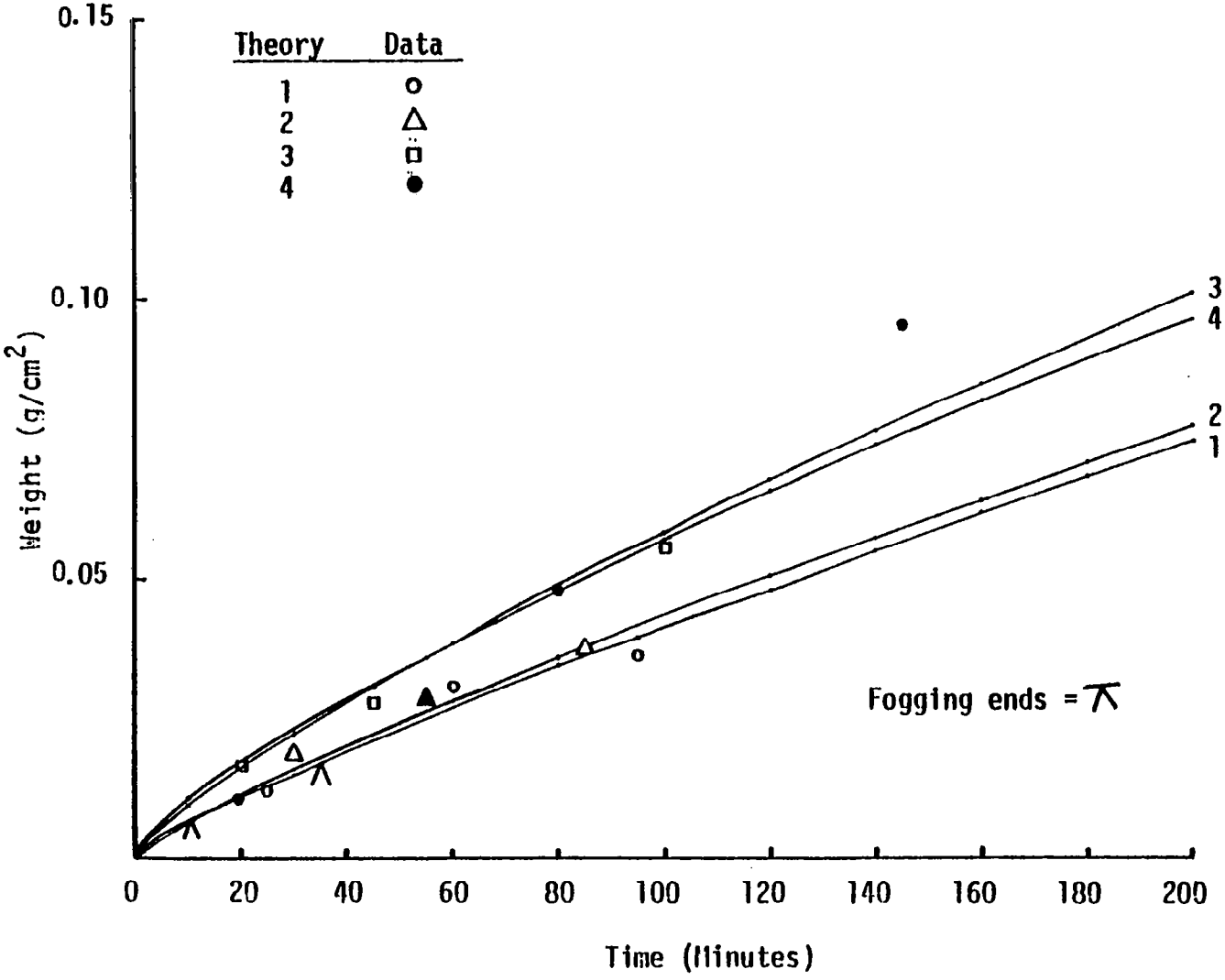

Figure 4. Frost Weight versus Time for Brian, et al. Data (Reference 2).

Then in Figure 4, we see that the frost weight is predicted very well. The Brian, et al. [1] data reported more measurements of frost thickness and weight. This time the smooth wall heat and mass transfer coefficients were increased by 1.27 rather than 2.24 due to the thermal entrance effects. The roughness effects increased the smooth wall heat transfer by 1.76 rather than 1.51 as in Brian, et al. [2]. The input data are shown in Table II and the corresponding frost thickness and weight comparisons are shown in Figures 5 and 6 respectively. There is less scatter in the frost thickness measurements and a very good prediction of the data. There is a similarly good result for the frost weight in Figure 6.

For the Yamakawa et al. reported measurements of frost thickness and weight, the input data are shown in Table III and the corresponding frost thickness and weight are shown in Figures 7 and 8 respectively. The curves 1, 2, and 4 in Figure 7 show good agreement with the frost thickness data, while curves 3 and 5 show the result of applying the water seepage model at the water seepage temperatures of 268.9°K. The water seepage model was applied in retrospect after evaluating other published data. A rule of thumb of determining when the water seepage model needs to be applied is in the observation of when the frost thickness data suddenly deviates from the basic predicted curve. A more direct method is to use an experimentor's own observations of cycling frost surface temperature, thus indicating water seepage effects. As more data is analyzed, the use of the water seepage model will become more objective. Lastly, Figure 8 shows good agreement of predictions with the data of the frost weight as a function of time.

The last example of frost formation in a duct with turbulent forced convection is from Jones and Parker. They only measured the frost thickness. No measurement was made of the frost weight or the heat and mass transfer coefficients. However, their apparatus and ambient conditions were similar

TABLE II
DATA INPUT TO THE FROST FORMATION MODEL FOR COMPARISON WITH BRIAN ET AL. [1] DATA FOR FORCED CONVECTION IN A DUCT

Computer Curve No.	Experimental Graph Symbol	Reynolds Number	Relative Humidity	Wall Temperature (°K)	Air Temperature (°K)
1	○	14500	26.1	79.83	297
2	△	9316	26.2	79.83	297
3	□	5603	26.0	79.83	297
4	●	14750	20.8	79.83	297
5	▲	9247	15.8	79.83	297
6	■	5625	16.2	79.83	297

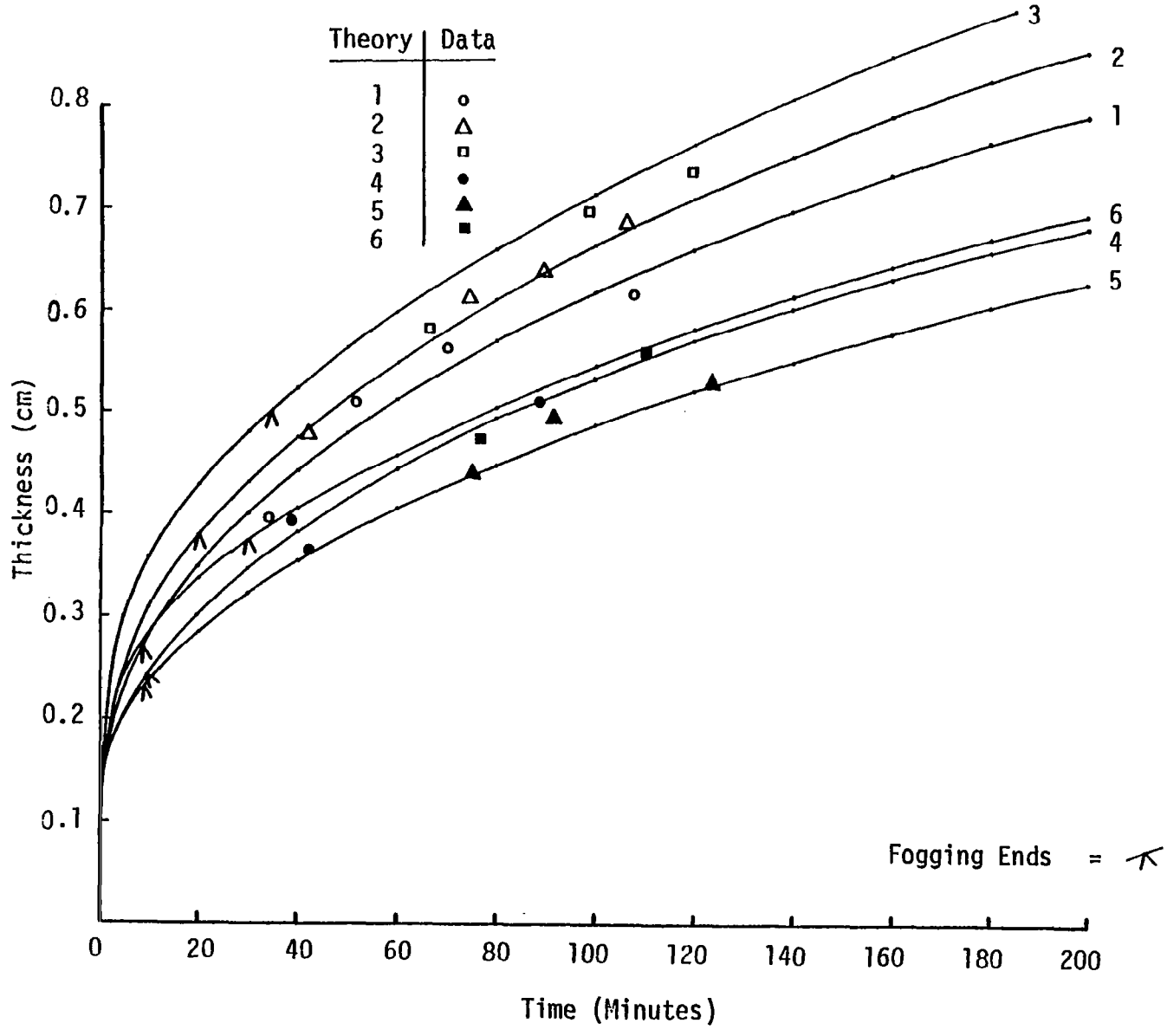

Figure 5. Thickness versus Time for Brian, et al. Data (Reference 1).

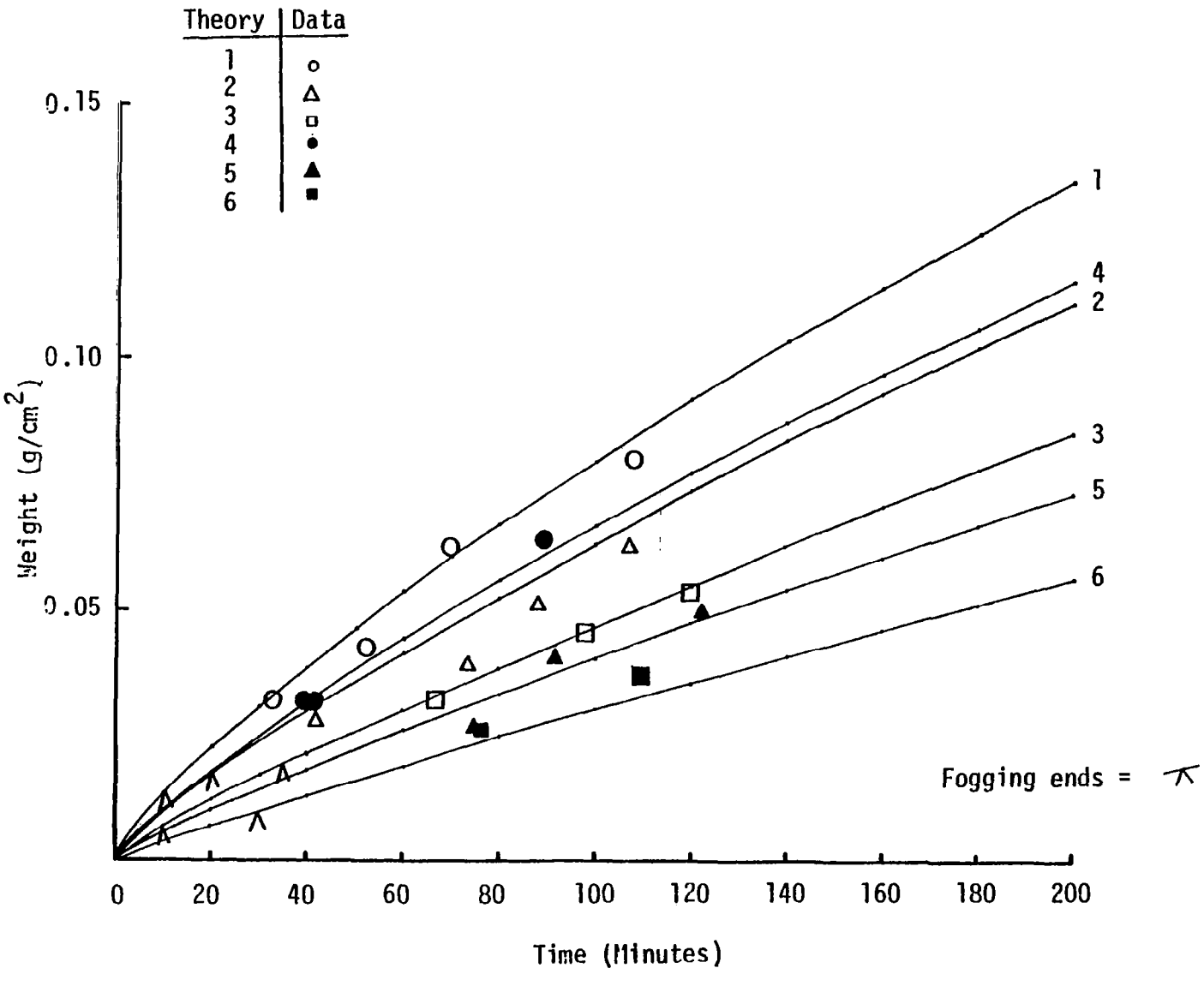

Figure 6. Frost Weight versus Time for Brian, et al. Data (Reference 1).

TABLE III
DATA INPUT TO THE FROST FORMATION MODEL FOR COMPARISON
WITH YAMAKAWA ET AL. [10] DATA FOR FORCED CONVECTION IN A DUCT

Computer Curve No.	Experimental Graph Symbol	Air Velocity (m/s)	Relative Humidity	Wall Temperature (°K)	Air Temperature (°K)
1	□	1.6	56.2	251	284
2	△	5.0	56.2	251	284
3	○	5.0	70.0	251	284
4	▲	7.3	56.2	251	284
5	●	7.3	97.4	251	284

Note: To calculate Reynolds Number, the hydraulic diameter is taken as $D_e = 20(1.7 - x_s)/(11.7 - x_s)$ cm.

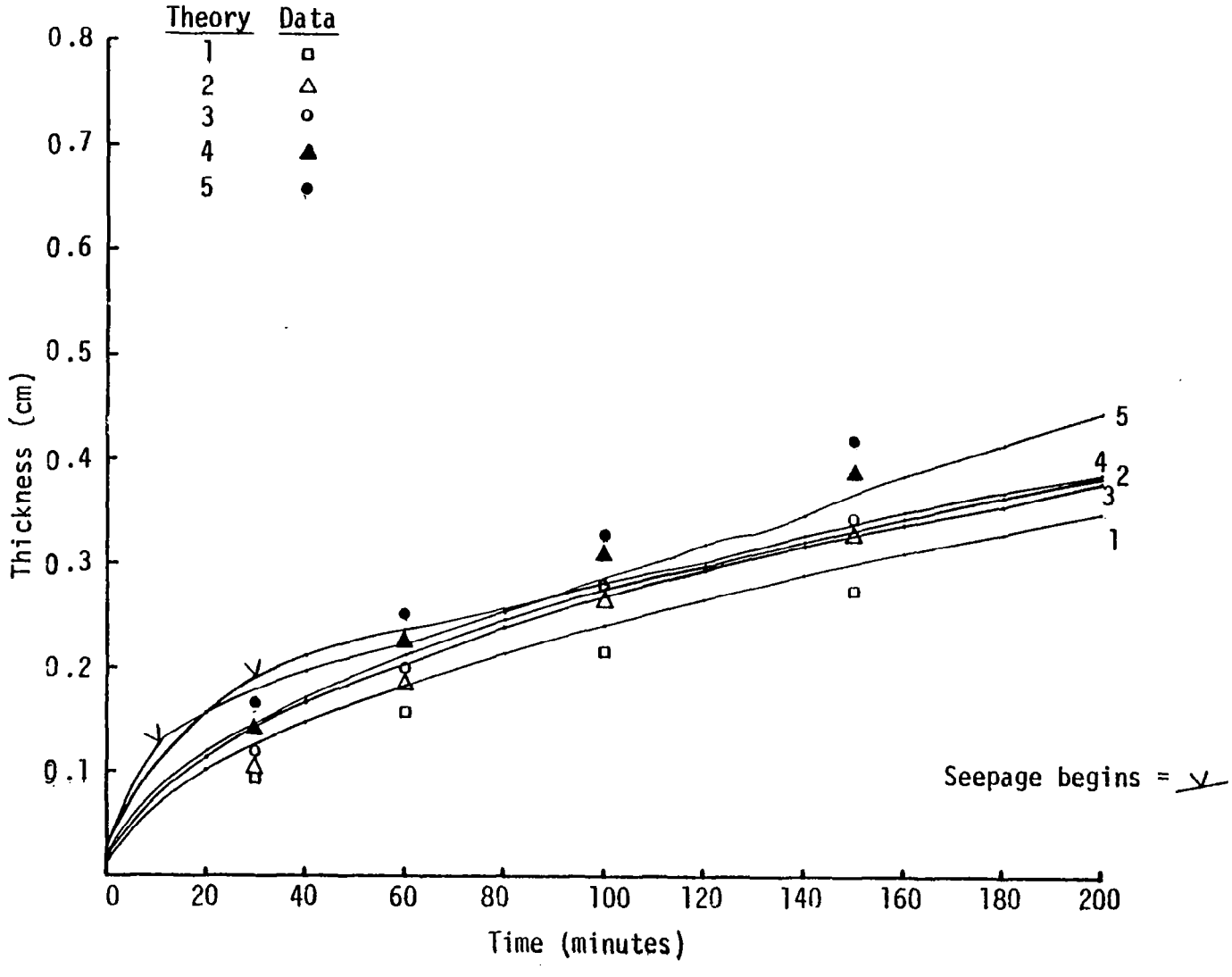

Figure 7. Frost Thickness versus Time for Yamakawa, et al. Data (Reference 10).

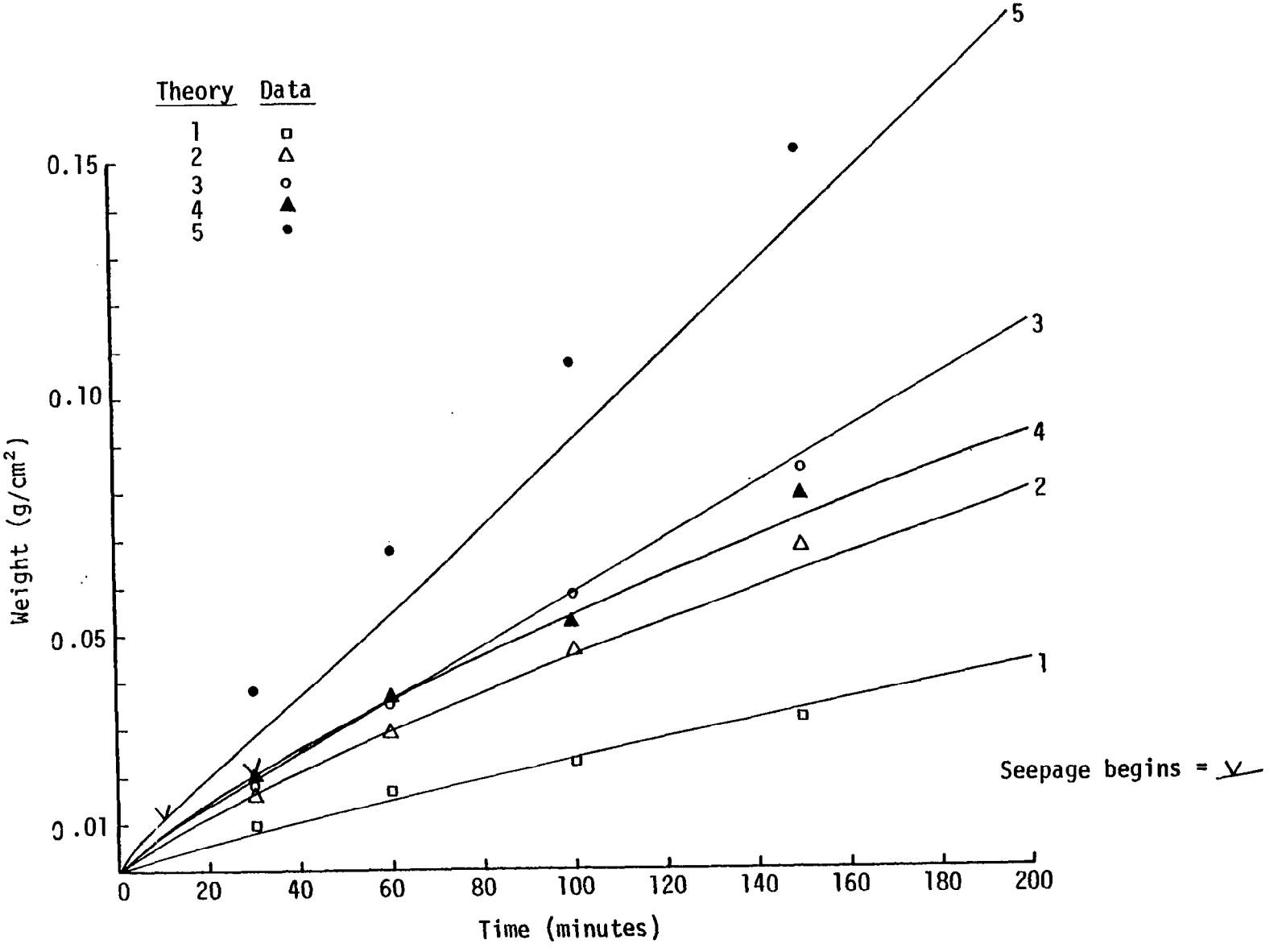

Figure 8. Frost Weight versus Time for Yamakawa, et al. Data (Reference 10).

enough to Yamakawa et al. that the correlations for the Nusselt and Sherwood numbers were extended to Jones and Parker's data as a best guess. Indeed, the Jones and Parker data warranted some attention because the ambient conditions were time-dependent, unlike other published data. The time-dependent ambient conditions are indicated in Table IV and the corresponding frost thicknesses in Figure 9. The very good comparison with the frost thickness data for the first sixty minutes prior to any ambient condition changes or any water seepage effects confirm the heat and mass transfer coefficient calculations. Curve 1 in Figure 9 shows a discontinuous change at 60 minutes as it should and continues to follow the data without the inclusion of water seepage effects. Curve 2 in Figure 9 also shows a dincontinuous change at 60 minutes and follows the data until 90 minutes without the use of the water seepage model. When a water seepage temperature of 268.7°K is used, good agreement is obtained from 75 minutes to 120 minutes. Curve 3, with a water seepage temperature of 272.0°K, is very interesting in that it levels out after 105 minutes just as the data does. Curve 4, with water seepage temperature of 269.3°K, shows a similar pattern to Curve 2 in predicting the data. The dashed lines show the effect of setting the water seepage temperature at the maximum possible value of 273.16°K. Thus the results are sensitive to selection of the water seepage temperature.

4.2 LAMINAR AND TURBULENT NATURAL CONVECTION ON A VERTICAL PLATE

The results from Nakamura [18] show that in laminar natural convection on vertical plates, the surface roughness has no effect on the heat transfer coefficient because the sensible heat flux from the air to the frost is mostly conductive, rather than convective. However, for natural convection, the momentum, heat and mass transfer mechanisms are coupled together in the boundary layer. The analysis for this problem is taken from Okino and

TABLE IV
DATA INPUT TO THE FROST FORMATION MODEL FOR COMPARISON
WITH JONES AND PARKER DATA [4] FOR FORCED CONVECTION IN A DUCT

Computer Curve No.	Experimental Graph Symbol	Air Velocity (m/s)	Absolute Humidity	Wall Temperature (°K)	Air Temperature (°K)	Time (minutes)
1	○	1.19	0.0070	255	296	0
1	○	1.19	0.0105	255	296	60
2	△	1.08	0.0095	255	304	0
2	△	1.08	0.0170	255	304	60
3	□	1.68	0.0093	258	298	0
3	□	3.02	0.0063	258	298	105
4	●	1.95	0.0075	259	298	0
4	●	1.95	0.0150	259	298	60

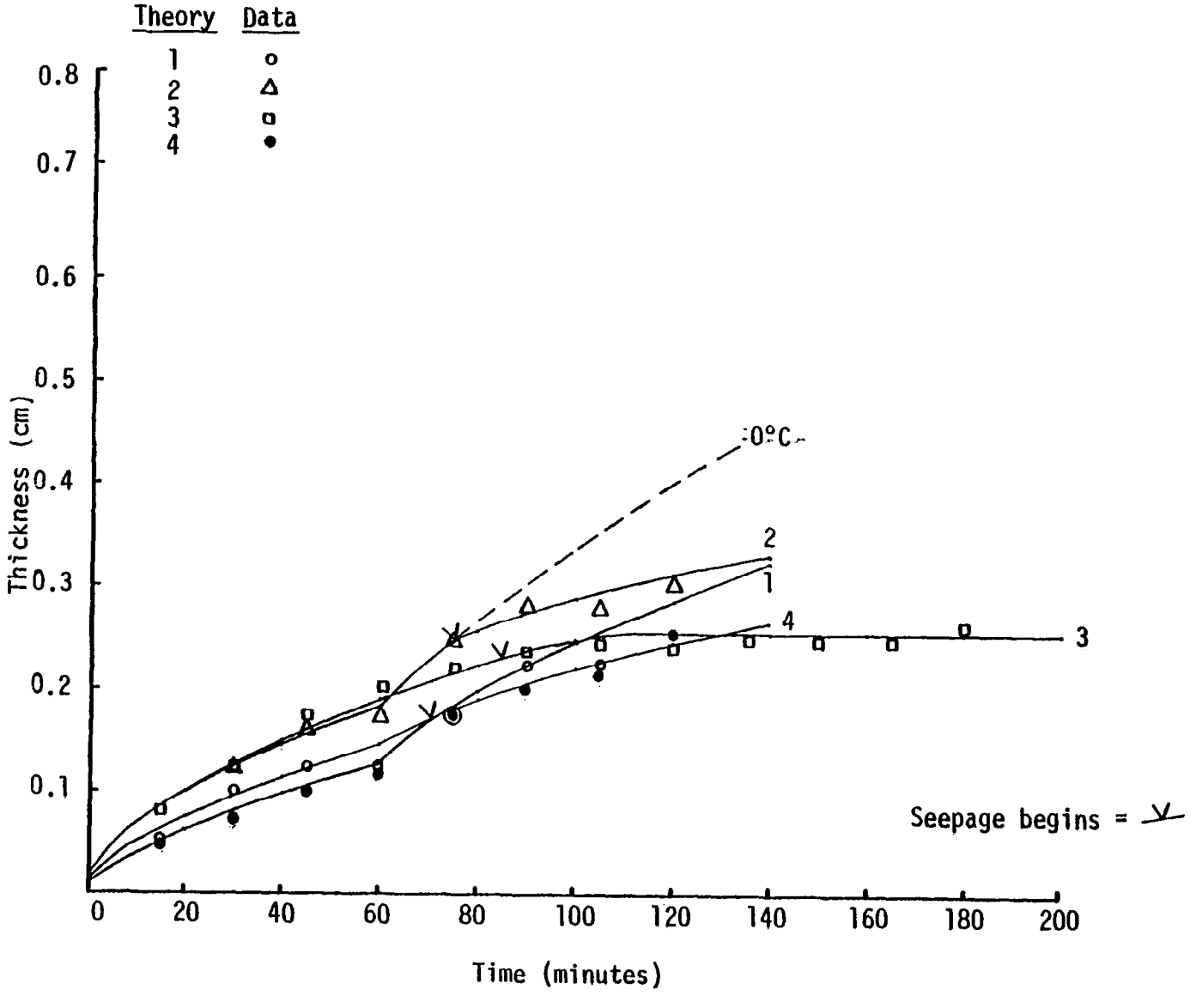

Figure 9. Frost Thickness versus Time for Jones and Parker Data (Reference 4).

Tajima [12] for a vertical plate under laminar natural convection. After correcting an algebraic error (the term $\sqrt{Sc}$ in η was placed in the denominator instead of the numerator in equation 23 below) in their analysis, the results are as follows,

$$Sh_H = \frac{h_m H}{\rho_a D} = \eta(1+\omega_s), \qquad Nu_H = \frac{h_H H}{k_a} = \eta/\xi \qquad (21),(22)$$

where

$$\eta = 2\sqrt{Sc \cdot \Phi} \left[\frac{Gr_H}{240\left[\frac{20}{21} + Sc\Phi\right]} \right]^{1/4} \qquad (23)$$

$$Gr_H = \frac{gH^3}{\nu^2} \left[\frac{\xi\ (T_a - T_s)}{T_a} + \frac{(\omega_a - \omega_s \Phi\ )}{(0.6453 + 2.6453\omega_a)} \right] \qquad (24)$$

$$\xi = \sqrt{\Phi^2 + 2\frac{Sc}{P_r}\Phi + 1} - \Phi \qquad (25)$$

$$\Phi = \frac{1 + \omega_a}{1 + \omega_s} \qquad (26)$$

The mean Nusselt and Sherwood numbers are

$$\overline{Nu}_H = \frac{4}{3}Nu_H , \qquad \overline{Sh}_H = \frac{4}{3}Sh_H \qquad (27),(28)$$

The Nusselt and Sherwood numbers (Nu_H and Sh_H) by these equations fitted Nakamura's data quite well.

Nu_H and Sh_H for turbulent flow, derived in Appendix III, are

$$Sh_H = 0.029791\ Sc^{7/15}\ \Phi^{1/5} \left[\frac{Gr_H}{1+0.49426\Phi Sc^{2/3}} \right]^{2/5} \qquad (29)$$

$$Nu_H = Sh_H\left(\frac{Pr}{Sc}\right)^{1/3} \qquad (30)$$

$$\xi = 1.875 - \sqrt{0.765625 + 4.08973\ \Phi\ \left[1-\left(\frac{Sc}{Pr}\right)^{2/3}\right]} \qquad (31)$$

The mean Nusselt and Sherwood numbers are

$$\overline{Sh}_H = \frac{5}{6}Sh_H\ , \qquad \overline{Nu}_H = \frac{5}{6}\ Nu_H \qquad (32),(33)$$

The Okino and Tajima [12] data show frost formations over time periods up to 20 hours, thus providing a severe test of the frost formation model. Frost was formed on vertical cylinders one meter in height. Frost thickness measurements were made at locations 0.1, 0.5, and 0.9 meters from the top. A comparison between equations (21) and (29) shows that the laminar flow occurs at 0.1 meters from the top and the turbulent flow occurs at 0.5 and 0.9 meters from the top, given the typical input values. The inputs into the frost formation model are shown in Table V and the corresponding frost thickness data from Okino and Tajima are reproduced in Figure 10. The curves 1, 2, and 3 (representing the different measurement locations) show a very good prediction of the frost thickness versus time. For these curves no phase three regime (including water seepage) occurred. For other test conditions, Okino and Tajima observed cyclic frost surface temperatures indicating water seepage. When curves 4 to 9 are examined we see there are three cycles of diffusional growth and water seepage growth. Curves 4, 5, 6, 7, 8, and 9 had the first water seepage temperatures at 268.3, 267.3, 267.3, 266.0, 264.6, and 265.4°K respectively. Thereafter the water seepage temperature was always increased by 1.2°K for successive cycles as corresponding to that observed by Okino and Tajima until 273.16°K was reached as a limit.

TABLE V
DATA INPUT TO THE FROST FORMATION MODEL FOR COMPARISON
WITH OKINO AND TAJIMA [11] DATA FOR NATURAL CONVECTION ON VERTICAL CYLINDER

Computer Curve No.	Experimental Graph Symbol	Plate Height (m)	Ambient Relative Humidity	Wall Temperature (°K)	Air Temperature (°K)
1	●	0.1	53	267.16	291.16
2	⊖	0.5	53	267.16	291.16
3	○	0.9	53	267.16	291.16
4	▲	0.1	64	263.16	292.16
5	◭	0.5	64	263.16	292.16
6	△	0.9	64	263.16	292.16
7	■	0.1	54	256.16	293.16
8	▣	0.5	54	256.16	293.16
9	□	0.9	54	256.16	293.16

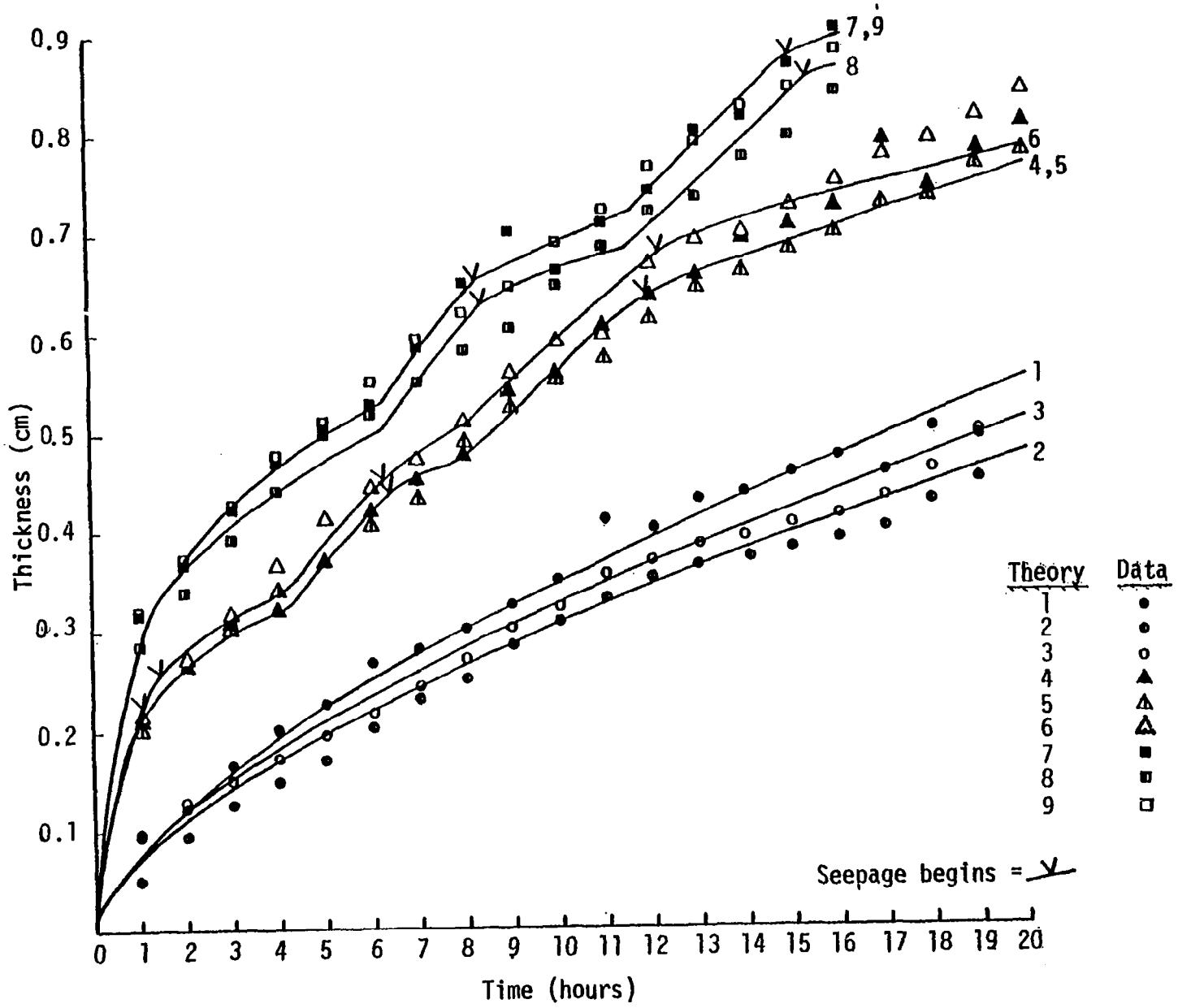

Figure 10. Frost Thickness versus Time for Okino and Tajima Data (Reference 11).

4.3 LAMINAR FORCED CONVECTION ON A CYLINDER

Both Schneider [9] and Andrichak [13] formed frost on a cylinder under laminar forced convection. Since Schneider observed that frost thickness did not vary around the cylinder circumference, and since he only reported frost thickness, a mean Nusselt number correlation was utilized from Fand and Keswani [19] as,

$$Nu_m\left(\frac{T_s}{T_a}\right)^{-0.17} = 0.184 + 0.324Re^{1/2} + 0.291Re^{X}, \qquad (34)$$

$$X = 0.247 + 0.0407Re^{0.168} \text{ for } 10^{-2} < Re < 2 \times 10^{5}$$

The Sherwood number was obtained via equation (18). The data input from Schneider is shown in Table VI and the corresponding frost thickness observations are shown in Figure 11. In all cases the water seepage temperature was set at 273.16°K. The curves 1 to 4 seem to indicate the water seepage model has the effect of making the frost thickness independent of the Reynold's number. Curve 5 predicts the data satisfactorily and curve 6 can be improved by using a water seepage temperature below 273.16°K. Schneider's correlation for the frost thickness (as shown by the dash lines) fits his own data quite well but does very poorly when applied to published data presented earlier in this paper. Schneider has several more frost thickness data, but all require water seepage temperature below freezing in order to obtain a proper fit with the data. Indeed, one can propose an empirical relationship for the water seepage temperature as a function of variables such as wall temperature, saturation ratio, etc. that would fit Schneider's frost thickness data as well as his correlation. The proposed empirical relationship should also be extended to other experimental data.

Andrichek has a sample of frost thickness measured near the stagnation and near the separation points of the cylinder, as

TABLE VI
DATA INPUT TO THE FROST FORMATION MODEL FOR COMPARISON
WITH SCHNEIDER DATA [8] FOR FORCED CONVECTION ON A CYLINDER

Computer Curve No.	Experimental Graph Symbol	Reynolds Number	Relative Humidity	Wall Temperature (°K)	Air Temperature (°K)
1	○	4000	0.96	268.16	278.16
2	△	8000	0.96	268.16	278.16
3	◇	16000	0.96	268.16	278.16
4	□	32000	0.96	268.16	278.16
5	⊞	32000	0.96	258.16	278.16
6	■	32000	0.96	248.16	278.16

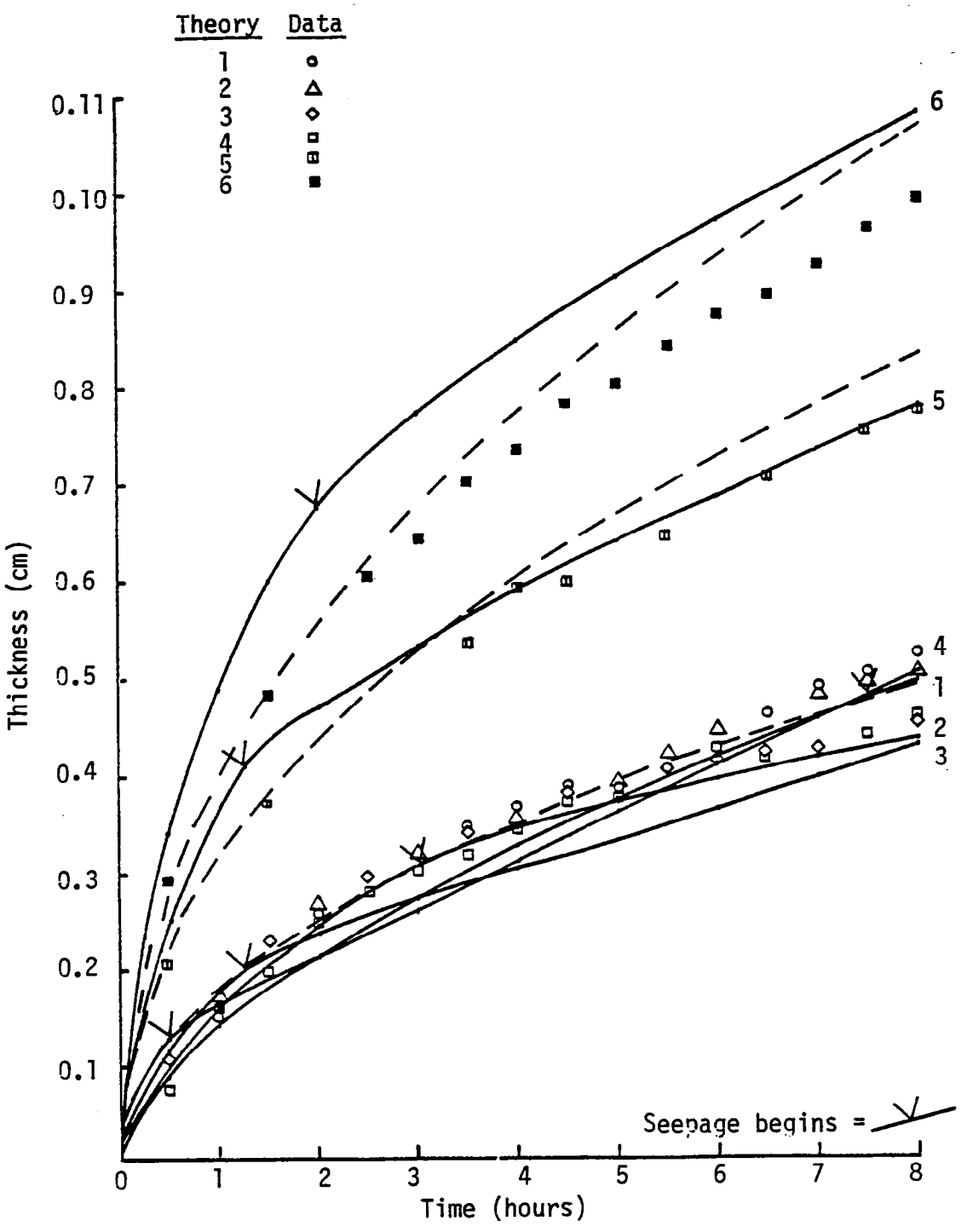

Figure 11. Frost Thickness versus Time for Schneider's Data (Reference 8).

shown in Figure 12. The local Nusselt number for laminar forced convection on a cylinder is,

$$Nu_D = 1.14 Pr^{0.4} \sqrt{Re_D \cos\theta} \quad . \tag{35}$$

Equation (35) is derived from the Handbook of Heat Transfer [14] and fits Nusselt number data presented in Schlichting [20] very well up to 80° from the stagnation line. The Sherwood number was obtained from Equation (18) as usual.

With the water seepage temperature set at 273.16°K it appears that curves 1 and 2 in Figure 12 predict the same frost thicknesses near stagnation and near separation. Very good agreement is made with the near separation data but only fair agreement with the near stagnation data. Yet, Schneider made a general observation that the frost thickness should not be a function of location on the cylinder. Thus the frost thickness distribution on the cylinder in forced convection remains somewhat unresolved.

4.4 LAMINAR AND TURBULENT FORCED CONVECTION ON A FLAT PLATE

In the last published data examined in this paper, White [10] used air suction through a horizontal duct with the frost formation on the upper duct surface. The heat and mass transfer coefficients were difficult to assess. For example, on some data sets it could not be determined whether the air flow was laminar or turbulent. Air suction in the duct made it difficult to decide between treating the geometry as a duct or as a flat plate. It was finally decided to treat the problem as a flat plate, and only accept those data that show good agreement with frost weight predictions. The Nusselt number for the laminar flat plate is given by

$$Nu_x = 0.332 \, Re_x^{1/2} Pr^{1/3} \tag{36}$$

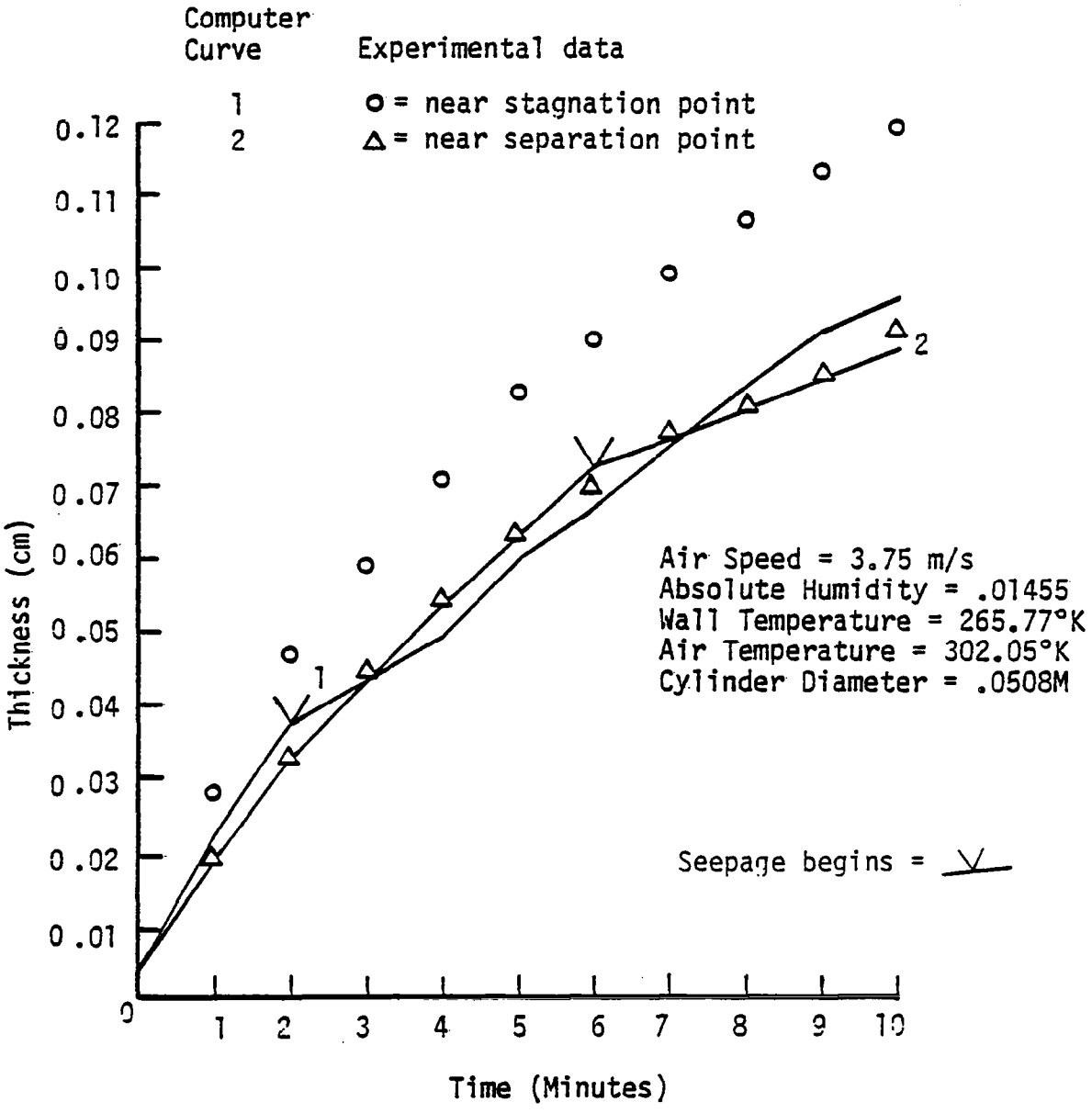

Figure 12. Frost Thickness versus Time for Andrichak Data (Reference 12). (See also Parish and Sepsy).

and for the turbulent flat plate given by a more complicated form,

$$Nu_x = St_x RePr, \tag{37}$$

$$\frac{C_f/2}{St_x} = 0.9 \left\{1 + 5\sqrt{\frac{C_f}{2}}\ 0.0897467 + \left(\frac{Pr}{0.9} - 1\right) + \ln\left[1 + \frac{5}{6}\left(\frac{Pr}{0.9} - 1\right)\right]\right\}, \tag{38}$$

and

$$C_f/2 = \frac{0.185}{(\log_{10} Re_x)^{2.584}} \tag{39}$$

as obtained from the Handbook of Heat Transfer.

The model input conditions for selected data from White are listed in Table VII and the corresponding frost thicknesses and weights are shown in Figures 13 and 14 respectively. We make special note of curve 4 for which the frost thickness and weight are predicted quite well. This is the only data obtained by White that did not exhibit water seepage. For the first three curves a water seepage temperature of 273.16°K was used. Of the first three curves, curve 1 provides the best prediction of frost thickness. Potentially, we can get good prediction of White's data providing we have good heat and mass transfer coefficients and good estimates for the water seepage temperatures below 273.16°K.

TABLE VII
DATA INPUT TO THE FROST FORMATION MODEL FOR COMPARISON
WITH WHITE [9] DATA FOR FORCED CONVECTION ON A FLAT PLATE

Computer Curve No.	Experimental Graph Symbol	Local Reynolds Number x 10^5 (Laminar or Turbulent)	Absolute Humidity	Wall Temperature (°K)	Air Temperature (°K)
1	△	T 2.50	0.00715	242.6	296.2
2	□	L 1.71	0.00762	247.1	296.6
3	▲	T 2.68	0.0152	248.1	295.9
4	■	T 2.25	0.0054	250.4	297.2

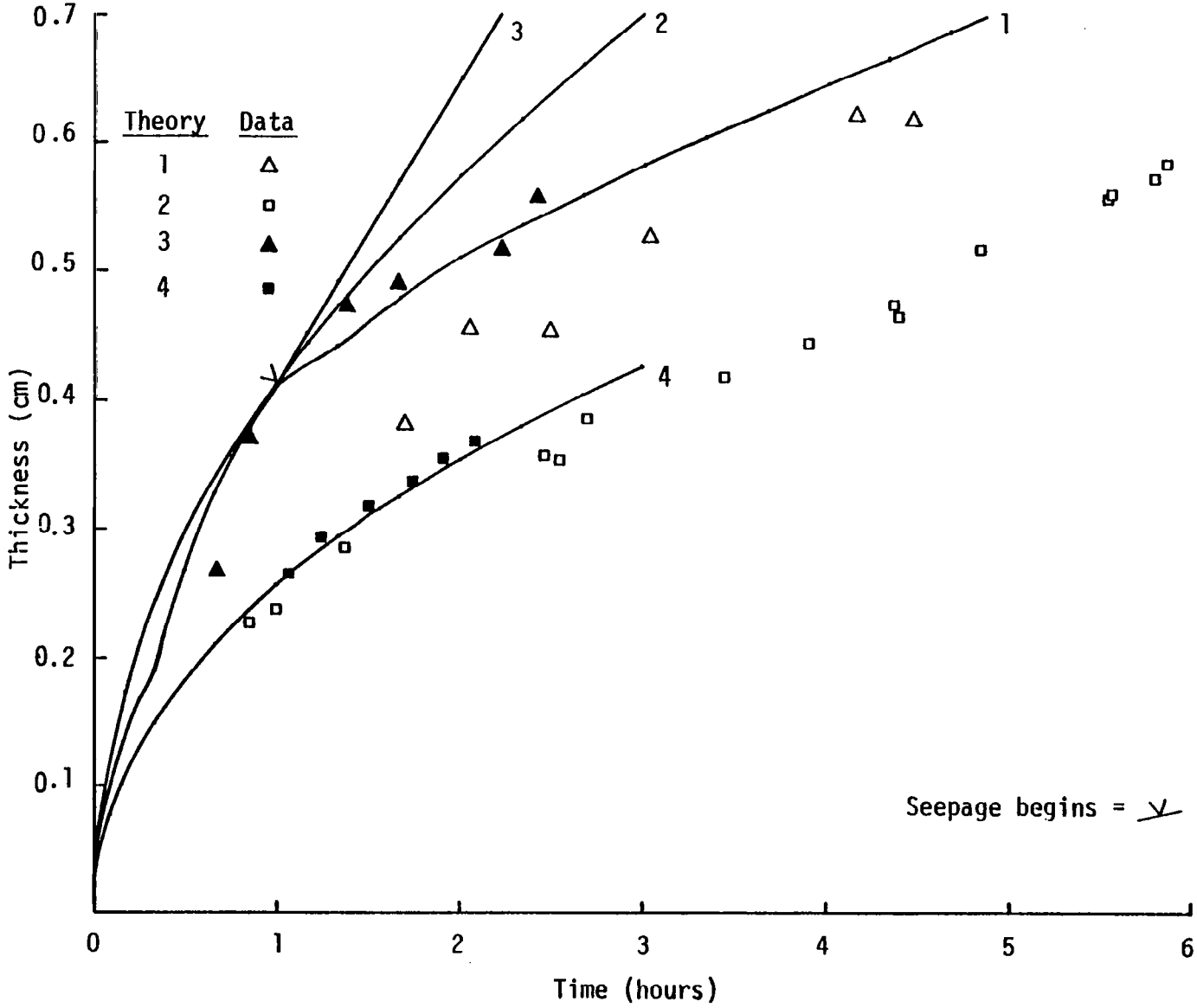

Figure 13. Frost Thickness versus Time for White's Data (Reference 9).

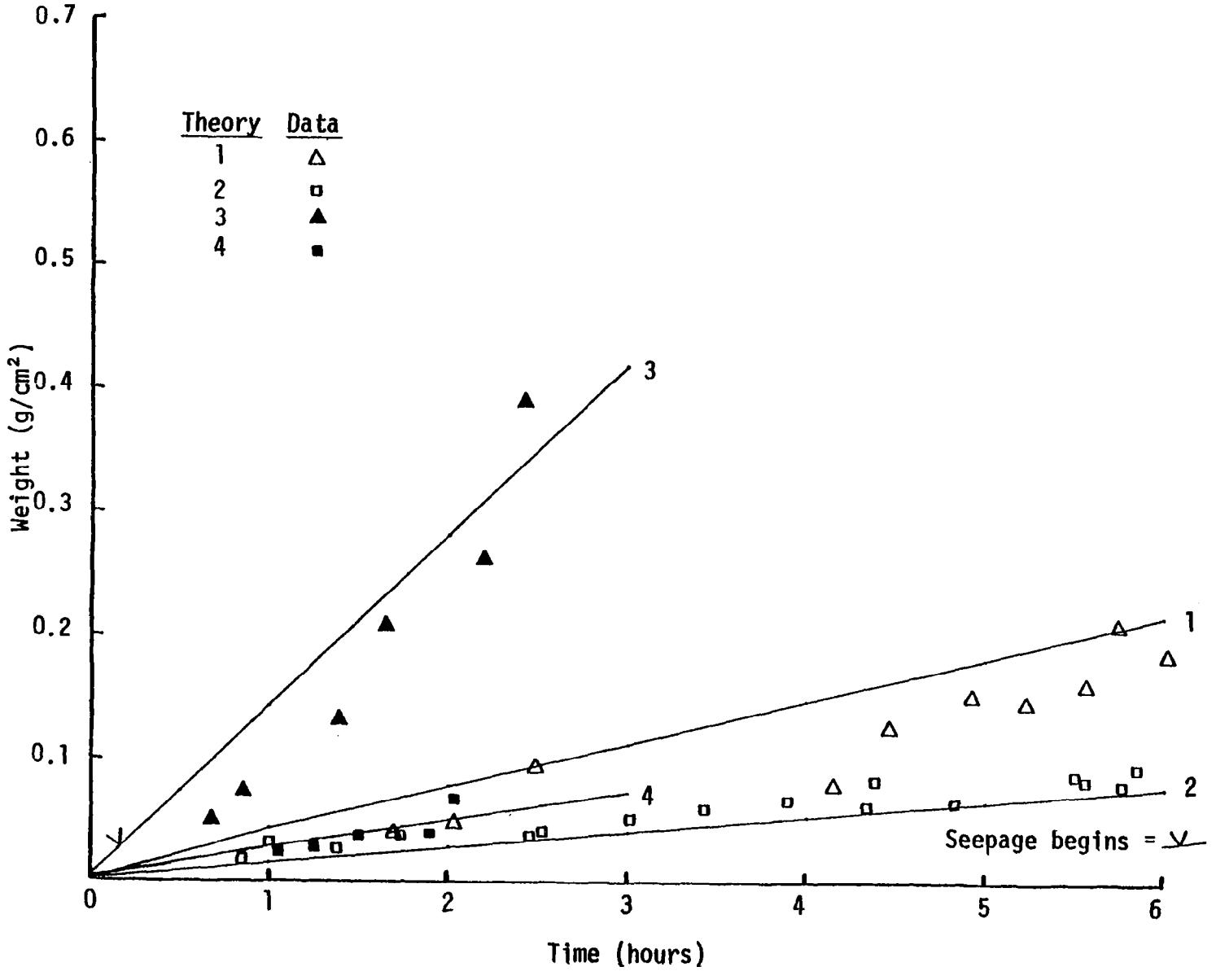

Figure 14. Frost Weight versus Time for White's Data (Reference 9).

SECTION 5
CONCLUSION

It was demonstrated in this paper that the basic approach by Brian et al.[1] has been improved to predict frost formation for other experimental data sets. Important enhancements included a generalized frost thermal conductivity and a water seepage model. Careful attention was given to deriving the heat and mass transfer coefficients for each particular data set. In particular, for turbulent forced convection in a duct the heat transfer coefficient was affected by the roughness of the frost layer and the mass transfer coefficient was affected by the boundary layer fogging. For natural convection it was determined that the heat, mass, and momentum transfer were coupled together, while the roughness effects were insignificant.

The success of its application to a diversity of flow regimes, geometrical shapes, time dependent ambient conditions, and long periods of time attest to the generality of the frost formation model. The frost formation model can be made even more general by devising an empirical relationship for the water seepage temperature and improving the estimates of the frost roughness height that can be used to calculate the heat transfer coefficients in turbulent flow. Eventually, the frost formation model will be further modified to calculate nocturnal frost formation on a wing section.

APPENDIX I
BOUNDARY LAYER FOGGING

If the temperature in the boundary layer falls below the dew point, it is possible for fog droplets to be nucleated. The occurance of such boundary layer fogging enhances the water vapor mass flux to the surface. The procedure followed for calculating this enhanced mass flux is outlined by Epstein [21]. The mass transfer coefficient in the presence of fogging is given by

$$h_m^* = h_m \frac{1 + C_p(T_a - T_s)/L_e(X_a - X_s)}{1 + \Delta \cdot C_p T_a / L_e X_a} \tag{40}$$

where

$$X = \frac{\rho_v}{\rho_v + \rho_a} \tag{41}$$

is the water vapor mass fraction and

$$\Delta = \frac{1}{T_a}\left[T_a - T_f + \frac{R_v T_f^2}{(L_e + 2.38)}\right] \tag{42}$$

The fog point temperature T_f is determined by solution of the equation

$$S \exp\left\{\frac{(L_e - 2.38)(T_a - T_f)}{R_v T_a T_f}\right\} = S_c\left[1 + \frac{(L_e - 2.38)(T_a - T_f)}{R_v T_f^2}\right] \tag{43}$$

where the critical saturation ratio for fog nucleation is approximated by the expression

$$\ell n S_c = 2.38/R_v T_a - 2.54 \tag{44}$$

Equation (40) is used for the mass transfer coefficient if the calculated value for T_f is such that $T_s < T_f < T_a$. The dew-point temperature equation is

$$T_d = \frac{T_a}{1 + \frac{R_v T_a}{L_e} \ln\left(\frac{1}{\phi_a}\right)} \tag{45}$$

where ϕ_a is the free stream relative humidity ratio.

APPENDIX II
FROST THERMAL CONDUCTIVITY

The frost thermal conductivity from Dietenberger [3] in capsule form is

$$K = 1/4\ \{(3B_c - 1)k_l + (3\theta_c - 1)k_u + \{[(3B_c - 1)k_l + (3\theta_c - 1)k_u]^2 + 8k_l k_u\}^{1/2}\} \quad . \tag{46}$$

The upper limit conductivity expression for air bubbles and ice cylinders is

$$k_u = (1 - B)k_b + Bk_c \text{(upper limit)} \tag{47}$$

where the thermal conductivity of air bubbles is given by:

$$k_b = k_i[1 - 2B(\frac{1 - a}{2 + a})]/[1 + B(\frac{1 - a}{2 + a})] \tag{48}$$

$$a = k_{eff\text{-}air}/k_i$$

and ice cylinders by:

$$k_c = (1 - B)k_i + Bk_{eff\text{-}air} \quad . \tag{49}$$

Likewise, the lower limit of thermal conductivity is formed by an interpolation between thermal conductivities for ice spheres and ice planes.

$$k_l = (1 - B)k_p + Bk_s \quad \text{(lower limit)} \tag{50}$$

where the thermal conductivity of ice spheres is given by:

$$k_s = k_i[3 + 2B(a - 1)]/[3 - B(\frac{a - 1}{a})] \tag{51}$$

and ice planes by:

$$k_p = \frac{k_i k_{eff\text{-}air}}{(1 - B)\ k_{eff\text{-}air} + k_i B} \tag{52}$$

B_c is the proportion of the frost volume representing ice spheres and ice planes given by,

$$B_c = 13.6(B_2 - B_1)(B - B_1)^2 \left[1 - \frac{2}{3}\left(\frac{B - B_1}{B_3 - B_1} + \frac{B - B_1}{B_2 - B_1}\right) + \frac{(B - B_1)^2}{2(B_3 - B_1)(B_2 - B_1)} \right] \left[1 + \frac{0.5264}{(\omega_a/\omega_w)} \right] \quad (53)$$

for $B > B_1$

$$B_c = 0 \text{ for } B \leq B_1 \quad (54)$$

$$B_1 = 0.1726\ (T/273.16), \quad (55)$$

$$B_2 = 0.751, \quad (56)$$

$$B_3 = B_2 + 0.3\sin\left[\left(\frac{\pi}{2}\right) \frac{1 - (T/273.16)^2}{1 - (T_w/273.16)^2} \right] . \quad (57)$$

The other portion of the frost volume representing ice cylinders and air bubbles is given by

$$\Theta_c = 1 - B_c . \quad (58)$$

The thermal conductivity of ice is given by

$$k_i = 630/T \quad (59)$$

and the effective thermal conductivity of air is given by,

$$k_{eff\text{-}air} = k_a + k_v \quad (60)$$

where

$$k_a = 2.646 \times 10^{-3} \left[\frac{T^{1/2}}{1 + \frac{245}{T}\, 10^{-12/T}} \right] \quad (61)$$

$$k_v = \frac{L_s D}{(1-\chi)} \left(\frac{P_v}{R_v T^2}\right)\left(\frac{L_s}{R_v T}\right) - 1 . \quad (62)$$

APPENDIX III

SOLUTION OF BOUNDARY-LAYER EQUATIONS FOR FREE CONVECTION TURBULENT FLOW

The integrated boundary-layer equations reproduced from Nakamura [18] for free convection are,

(a) Momentum Equation

$$\frac{d}{dx}\left[\int_o^{\delta} \rho u^2 dy\right] = -\tau_w + \int_o^{\delta} (\rho - \rho_\infty) g \cos\phi dy \qquad (63)$$

(b) Energy Equation

$$\frac{d}{dx}\left[\int_o^{\delta_t} \rho u c_p (T - T_\infty) dy\right] = j_{qw} + \rho V_w C_p (T_w - T_\infty) \qquad (64)$$

(c) Diffusion Equation

$$\frac{d}{dx}\left[\int_o^{\delta} \rho u (X_1 - X_{1\infty}) dy\right] = j_{1w} + \rho V_w (X_{1w} - X_{1\infty}) \qquad (65)$$

(d) Normal velocity at the frost surface (zero net flow of air)

$$V_w = \frac{j_{1w}}{\rho(1 - X_{1w})} \qquad (66)$$

Barron and Han [22] show the same equations with one important subtle difference. Barron and Han assumed the thermal thickness is the same as the momentum thickness, δ, and the diffusional thickness is different from the momentum thickness. Nakamura [18] and Skelland [23] assumed that the diffusional thickness is the same as the momentum thickness and the thermal thickness is different from the momentum thickness. We chose the latter approach for the reason explained later. Barron and Han demonstrated the effect of thermal diffusion as nil, thus simplifying the equations somewhat. The integrals were evaluated using the following velocity, temperature and mass fraction profiles from Skelland and Barron and Han as

$$\frac{U}{U_m} = \left(\frac{Y}{\delta}\right)^{1/7} \left(1 - \frac{Y}{\delta}\right)^{4} , \tag{67}$$

$$\Theta = \frac{T - T_\infty}{T_w - T_\infty} = 1 - \left(\frac{Y}{\delta_t}\right)^{1/7} , \tag{68}$$

$$\phi = X_1 - X_{1\infty} = \left[1 - \left(\frac{Y}{\delta}\right)^{1/7}\right] \left(X_{1w} - X_{1\infty}\right) \tag{69}$$

where

$$U_m = c_1 X^{1/2} , \tag{70}$$

$$\delta = c_2 X^{7/10} , \tag{71}$$

$$\xi = \delta_t/\delta , \quad \text{and} \tag{72}$$

$$\frac{\rho - \rho_\infty}{\rho_\infty} = -B_t(T - T_\infty) - B_m(X_1 - X_{1\infty}) \tag{73}$$

$$B_t = \frac{1}{T_\infty} \quad \text{and} \quad B_m = \frac{0.6078}{1 + 0.6078X_{1\infty}} \tag{74),(75}$$

From Skelland the surface shear stress was

$$T_o = 0.0228\rho\left(\frac{U_m^{\,2}}{g_c}\right)\left(\frac{\nu}{U_m \delta}\right)^{1/4} . \tag{76}$$

Then the Colburn's analogy was used to get the heat and mass transfer equations as,

$$j_{1w}/T_o g_c = \frac{X_{1w} - X_{1\infty}}{Sc^{2/3} U_m} , \quad \text{and} \tag{77}$$

$$j_{qw}/T_o g_c = \frac{c_p(T_w - T_\infty)}{Pr^{2/3} U_m} \tag{78}$$

Substituting all the previous equations into equations (63), (64), and (65) the following result is obtained,

$$C_1^2 0.088935 = \frac{g \cos\phi}{8} \left[\xi B_t (T_\infty - T_w) + B_m (X_{1\infty} - X_{1w})\right]$$

$$-0.0228 \nu^{1/4} \left(\frac{C_1^7}{C_2^5}\right)^{1/4} \tag{79}$$

$$C_1^{1/4} C_2^{5/4} \frac{6}{5} \left\{\xi^{8/7}\left(\frac{7}{8} - \frac{7}{9}\right) - \xi^{15/7}\left(\frac{28}{15} - \frac{28}{16}\right) + \xi^{22/7}\left(\frac{42}{22} - \frac{42}{23}\right)\right.$$

$$\left. - \xi^{29/7}\left(\frac{28}{29} - \frac{28}{30}\right) + \xi^{36/7}\left(\frac{7}{36} - \frac{7}{37}\right)\right\}$$

$$= \left(\frac{1}{Pr^{2/3}} + \frac{X_{1w} - X_{1\infty}}{Sc^{2/3}(1 - X_{1w})}\right)\left(0.0228 \nu^{1/4}\right) \tag{80}$$

$$C_1^{1/4} C_2^{5/4} \frac{6}{5}(0.03663)$$

$$= \left(\frac{1 - X_{1\infty}}{1 - X_{1w}}\right)\left(\frac{1}{Sc^{2/3}}\right)(0.0228 \nu)^{1/4} \tag{81}$$

The solution for ξ is obtained from combining equations (80) and (81) and doing a parabolic Taylor's expansion of the terms containing about $\xi = 1$ to get equation (31) in the text.

The values for C_1 and C_2 are solved from combining equations (79) and (80) which then lead us to the equations, for δ and U_m as,

$$\frac{\delta}{x} = 0.57167 \left(\frac{1 - X_{1w}}{1 - X_{1\infty}}\right)^{-0.8} Gr_x^{-0.1} Sc^{-8/15}$$

$$\left(1 + 0.4943 \left(\frac{1 - X_{1w}}{1 - X_{1\infty}}\right) Sc^{2/3}\right)^{0.1} \tag{82}$$

and $$U_m = 1.1855 \left(\frac{\nu}{x}\right) Gr_x^{1/2} \left(1 + 0.4943 \left(\frac{1-X_{1w}}{1 - X_{1\infty}}\right) Sc^{2/3}\right)^{-1/2} \tag{83}$$

where Gr_x is given by equation (24) in the text and

$$\Phi = \frac{1 - X_{1w}}{1 - X_{1\infty}} = \frac{1 + \omega_a}{1 + \omega_s} \quad , \quad \frac{1}{1 - X_{1w}} = 1 + \omega_w \quad , \quad H = x. \qquad (84)$$

The Sherwood and the Nusselt numbers are defined by

$$Sh_x = \frac{j_{1w}x}{(X_{1w} - X_{1\infty})\rho D} \qquad \text{and} \qquad Nu_x = \frac{j_{qw}x}{(T_w - T_\infty)k_a} \qquad (85),(86)$$

which when combined with equations (76), (77), (78), (82), and (83) give the equations (29) and (30) in the text for the local Sherwood and Nusselt numbers. As a result we obtained the Chilton-Colburn analogy given by equation (30) as should happen when using Colburn's equations for the heat and mass transfer. Barron and Han derived a different analogy result than the Chilton-Colburn analogy, thus invalidating their own results.

To evaluate the roughness effects on the heat transfer coefficient in turbulent flow the friction velocity, U_T, obtained from the stress equation (76) at a one-meter height for typical conditions was combined with the typical frost thickness to show that the roughness Reynolds number, $U_T k_s/\nu$ was around 5 to 25, thus indicating a smooth wall behavior for the Okino and Tajima data.

REFERENCES

1. Brian, P. L. T., Reid, R. C. and Brazinsky, F., "Cryogenic Frost Properties," Cryogenic Technology, Sept./Oct. 1979.

2. Brian, P. L. T., Reid, R. C., and Shah, Y. T., "Frost Deposition on Cold Surfaces," J. Eng. Chem. Fundamentals, Vol. 9, 1970.

3. Dietenberger, M. A., "Generalized Correlation of the Water Frost Thermal Conductivity," to be published in International J. of Heat and Mass Transfer.

4. Chen, M. M. and Rohsenow, W., "Heat, Mass, and Momentum Transfer Inside Frosted Tubes - Experiment and Theory," ASME Journal of Heat Transfer, August 1964, pg 334-340.

5. Jones, B. W. and Parker, J. D., "Frost Formation with Varying Environmetnal Parameters", ASME Journal of Heat Transfer, May 1975, pp.255-259.

6. Biguria, G. and Wenzel, L. A., "Measurement and Correlation of Water Thermal Conductivity and Density," Vol. 9, No. 1, I & EC Fundamentals, February 1970, p. 129.

7. Lotz, H., "Heat and Mass Transfer Processes in Air Radiators with Laminated Fins Covered with Frost in Relation to Their Operating Behavior," Ira German, p. 208, Kaltetechnik-Klimatisierung. 23, Jahrgang. Heft 7/1971.

8. Parish, H. C. and Sepsy, C. F., "A Numerical Analysis of Frost Formation Under Forced Convection," ASHRAE Paper No. 2231 presented at ASHRAE Semiannual Meeting, New Orleans, LA., Jan. 23-28, 1972

9. Schneider, H. W., "Equation of the Growth Rate of Frost Forming on Cooled Surfaces," Int. J. Heat Mass Transfer. Vol. 21, 1978, pp. 1019-1024.

10. White, J., "Heat and Mass Transfer in Thick Frost Layers," Ph.D. dissertation, University of Kentucky, Mechanical Engineering Department, 1973.

11. Yamakawa, N., Takahashi, N. and Ohtani, S., "Forced Convection Heat and Mass Transfer Under Frost Conditions," Heat Transfer - Japanese Research, Vol. 1, No. 2, 1972.

12. Okino,Y. and Tajima, O., "Heat and Mass Transfer by Free Convection Under Frosting Conditions," Translated by Osamu Tajima, originally published in Reito, 48, p. 338-349, 1973.

13. Andrichak, S. M., "Formation of a Layer of Frost on a Cylinder in Crossflow of Air," the Ohio State University, 1962.

14. Rohsenow, N. M. and Hartnett, J. P., Handbook of Heat Transfer, McGraw-Hill Book Company, 1973.

15. Langston, P. A. S., "Hoar Frost on Aircraft Surfaces," BEA Engineering - Project and Development Technical Note No. P/570, Nov. 18, 1968.

16. Street, R. L., "Turbulent Heat and Mass Transfers Across a Rough, Air-Water Interface: A Simple Theory," Int. J. Heat Mass Transfer, Vol. 22, pp. 885-899, 1979.

17. Yaglom, A. M. and Kader, B. A., "Heat and Mass Transfer Between a Rough Wall and Turbulent Fluid Flow at High Reynolds and Peclet Numbers," J. Fluid Mech. (1974) Vol. 12, part 3, pp. 601-623.

18. Nakamura, H., "Free Convective Heat Transfer From Humid Air to a Vertical Plate Under Frosting Conditions," Bull. JSME Vol. 17, 1974.

19. Fand, R. M. and Keswani, K. K., "A Continuous Correlation Equation for Heat Transfer From Cylinders to Air in Crossflow for Reynolds Numbers From 10^{-2} to 2×10^{5}," Int. J. Heat Mass Transfer, Vol. 15, pp. 559-562, 1972.

20. Schlichting, H., Boundary Layer Theory, McGraw-Hill Book Company, 1960, p. 320.

21. Epstein, M., "Nonequilibrium Fog Formation Within the Thermal Boundary Layer," Ph.D. Thesis in the Mechanical Engineering Department at Polytechnic Institute of Brooklyn, June 1969.

22. Barron, R. F. and Han, L. S., "Heat and Mass Transfer to a Cryosurface in Free Convection," ASME Journal of Heat Transfer, November, 1965, pp. 499-506.

23. Skelland, A. H. P., Diffusional Mass Transfer, John Wiley & Sons, Inc., 1974, p. 225.

TECHNICAL REPORT STANDARD TITLE PAGE

1. REPORT NO.	2. GOVERNMENT ACCESSION NO.	3. RECIPIENT'S CATALOG NO.
NASA CR-3595		

4. TITLE AND SUBTITLE	5. REPORT DATE
A Frost Formation Model and Its Validation Under Various Experimental Conditions	August 1982
	6. PERFORMING ORGANIZATION CODE
7. AUTHOR(S)	8. PERFORMING ORGANIZATION REPORT #
Mark A. Dietenberger	
9. PERFORMING ORGANIZATION NAME AND ADDRESS	10. WORK UNIT NO.
Applied Systems Analysis Section University of Dayton Research Institute Dayton, Ohio 45469	M-386
	11. CONTRACT OR GRANT NO. NAS8-33369
12. SPONSORING AGENCY NAME AND ADDRESS	13. TYPE OF REPORT & PERIOD COVERED
National Aeronautics and Space Administration Washington, D.C. 20546	Contractor Report
	14. SPONSORING AGENCY CODE

15. SUPPLEMENTARY NOTES

Marshall Technical Monitor: Dennis Camp
Final Report

16. ABSTRACT

A general frost formation model was developed to calculate the frost weight and thickness on a cold isothermal surface subjected to varying environmental parameters. The restrictions of limited frost density and temperature ranges were essentially removed by development of a generalized correlation of the water frost thermal conductivity. The diffusional approach used by Brian, et al. was extended to include the full range of frost density and temperatures and to include the water seepage phase of frost growth. Careful attention was given to the heat and mass transfer coefficients for a given air flow regime and geometrical shape. The extended frost formation model was successful in predicting the frost growth for various published data.

17. KEY WORDS	18. DISTRIBUTION STATEMENT
Frost Frost modeling Aviation safety	Unclassified - Unlimited Subject Category 47

19. SECURITY CLASSIF. (of this report)	20. SECURITY CLASSIF. (of this page)	21. NO. OF PAGES	22. PRICE
Unclassified	Unclassified	68	A04

MSFC - Form 3292 (Rev. December 1972)

For sale by National Technical Information Service, Springfield, Virginia 22161

NASA-Langley, 1982